MODELING OF ARTERIAL HEMODYNAMICS

by

Jonathan Edwards

A thesis submitted to the Faculty of the University of Delaware in partial fulfillment of the requirements for the degree of Master of Science in Biomechanics and Movement Science

Fall 2009

MODELING OF ARTERIAL HEMODYNAMICS

by

Jonathan Edwards

Approved: _____
William C. Rose, Ph.D.
Professor in charge of thesis on behalf of the Advisory Committee

Approved: _____
Lynn Snyder-Mackler, Ph.D.
Chair of the Biomechanics and Movement Sciences Program

Approved: _____
James G. Richards, Ph.D.
Deputy Dean of the College of Health Sciences

Approved: _____
Debra Hess Norris, M.S.
Vice Provost for Graduate and Professional Education

ACKNOWLEDGEMENTS

I thank Justin Spaeth and Prof. Antony Beris for sharing an early version of the modeling software, which came from Justin's undergraduate thesis work, with Dr. Rose. I thank Dr. Edwards and Dr. Farquhar for the use of their lab space, their equipment, their supplies, and their advice and expertise. I thank my committee: Dr. Edwards, Dr. Knight, and Dr. Rose for their help and dedication. I thank my fellow graduate student colleagues for being great friends. I thank my advisor, Dr. Rose, for his patience and care; I could not have wished for a better mentor, and more importantly, companion. Finally, I thank my family for their support and love.

This work was supported by funding from the Department of Health, Nutrition, and Exercise Sciences to William Rose.

TABLE OF CONTENTS

LIST OF TABLES

LIST OF FIGURES

ABSTRACT

Accurate noninvasive measurement of the blood pressure waveforms throughout the body is clinically desirable, but difficult to accomplish. We use a computational model, based on a description of the architecture and mechanical properties of the arterial network and blood, to predict dynamic pressure throughout the arterial vasculature. Applanation tonometry was used to measure dynamic pressure noninvasively at the carotid, radial, and femoral arteries under different hemodynamic conditions (baseline, cold pressor test, and nitroglycerin). A pressure waveform from one recording site served as input to the model. Model parameters were adjusted to obtain the best fit between the pressures predicted at other locations and the pressures directly measured at those locations. The site whose pressure was used as the input was altered, and the ability to accurately predict pressures at the other sites was compared.

In twenty one healthy subjects, the femoral and radial artery pressures have allowed most accurate prediction of pressures elsewhere. Vascular stiffness, resistance, and the dependence of stiffness on arterial diameter were estimated from the fitted model parameters. The model provides insight into the effects of physiological and pharmacological stimulation on arterial vascular properties in vivo. The model also provides a noninvasive estimate of central aortic pressure, which is valuable for understanding ventricular-vascular coupling in health and disease.

Chapter 1

INTRODUCTION

Cardiovascular disease (CVD) is a leading cause of death around the world. In the United States, heart disease claims over 650 thousand lives (comprising 27% of all deaths) annually, and is the leading cause of death (Center for Disease Control and Prevention). Due to the prevalence of CVD, much research has focused on understanding the cardiovascular system.

Structural and functional arterial wall changes precede the development of coronary artery disease (CAD) (Ross, 1981). A large study (Laurent, et al., 2001) found that in 1980 hypertensive patients, artery stiffness was strongly correlated with mortality risk. Specifically, a 5 m/s increase in pulse-wave velocity corresponded to a 34% increase in all-cause mortality risk, a 51% increase in CVD mortality risk, and the equivalent mortality risk of aging 10 years. (Pulse wave velocity is an indirect measure of arterial stiffness, according to the Bramwell-Hill equation which relates the two (McDonald DA, 1974).) Further, increased arterial stiffness is associated with left ventricular hypertrophy (Girerd, 1991), which is a known risk factor for cardiovascular events (Levy, Garrison, Savage, Kannel, & Castelli, 1990). It has also been observed (Cohn, et al., 1995) that there is a 31% reduction in arterial oscillatory compliance in hypertensive individuals, and a reduction in systemic functional oscillatory compliance,

in patients with CAD. These results suggest that accurate measurement of arterial compliance may allow for the early detection of vascular disease.

The magnitude and timing of wave reflection also plays a critical role in cardiovascular functioning, particularly in the coupling between the heart and blood vessels. The input impedance of the canine circulation was measured (O'Rourke & Taylor, 1967) and explained by the authors in terms of wave reflection from upper and lower body reflecting sites. Nichols et al., 1985, showed that age-related changes in ventricular-vascular coupling have been explained in terms of changes in wave reflection, with older patients having increased pulse wave velocity and increased wave reflection, as well as decreased stroke volume and decreased cardiac output (Nichols, O'Rourke, Yaginuma, Murgo, Pepine, & Conti, 1985). The CAFE study (Williams, et al., 2006) followed over 2000 hypertensive patients randomly assigned to drug therapy with a beta blocker or a calcium channel blocker (CCB). The patients on a CCB had fewer cardiovascular events and were less likely to develop renal impairment than those receiving a β blocker, even though both groups had statistically equal reductions in brachial cuff pressures. Estimated central aortic pressure, which differs from brachial pressure due to the effects of wave reflection, was not the same in the two groups: the patients on CCBs had lower aortic systolic pressures and lower aortic pulse pressures than the patients on β blockers. This indicates that the effects of wave reflection are significant and clinically relevant, and that brachial cuff pressure alone may not be sufficient to fully account for the different clinical results obtained with different forms of treatment. Augmentation index is used to quantify the contribution of the reflected

pressure wave to systolic pressure, and can be determined non-invasively by tonometry (Nichols, 2005). Enhanced external counterpulsation therapy, used to help patients with angina who do not respond to conventional treatment, was shown to cause a decrease in augmentation index (i.e. less of an increase in systolic pressure due to wave reflection) and an increase in reflected wave travel time, and this difference correlated with less frequent and less severe angina (Nichols, Estrada, Braith, Owens, & Conti, 2006). This is further evidence of the clinical importance of wave reflection in the cardiovascular system.

Current clinical practice relies on a cuff sphygmomanometer to measure brachial artery systolic and diastolic pressure noninvasively. However, because this technique is performed on a peripheral artery, and because it only provides the maximum and minimum pressures, it gives incomplete information about central hemodynamic functioning, as demonstrated by the CAFÉ study mentioned earlier (Williams, et al., 2006) and various other studies, summarized and reviewed by Nichols and Edwards (Nichols & Edwards, 2001).

One approach to estimating central aortic blood pressure is to mathematically transform peripheral pressure into central pressure. In 1997, a transfer function was validated that could accurately ($\leq 0.2 \pm 3.8$ mmHg error) predict a central aortic pressure waveform from a radial waveform collected by applanation tonometry. One limitation of this transfer function was that the reconstructed aortic pressure waveform tended to

underestimate the AI, attributable to the high fidelity of the wave shape necessary to estimate the contribution of wave reflection (Chen, et al., 1997).

A transfer function is dependent on its method of derivation. The transfer function derived by Chen, et al., 1997, was developed using an auto-regressive (AR) model. A transfer function may also be derived from a Fourier analysis. In 1999, the performance of these two methods was compared. The transfer function derived from the AR model was superior, containing less noise and more stability (Fetics, Nevo, Chen, & Kass, 1999). Today, the commercially available Sphygmocor system relies on this AR modeling approach. Equation 1 describes the transfer function method quantitatively.

$$p_{rad}(t) \xrightarrow{F.T.} P_{rad}(f) \tag{1a}$$

$$P_{rad}(f) \ x \ TF(f) = P_{ao}(f)_{predicted} \tag{1b}$$

$$P_{ao}(f)_{predicted} \xrightarrow{I.F.T.} p_{ao}(t)_{predicted} \tag{1c}$$

In Equation 1, P_{rad} (p_{rad}) and P_{ao} (p_{ao}) represent the radial and aortic pressures in the frequency (or time) domain, respectively, (t) and (f) refer to the time and frequency domains, respectively, and $F.T.$ and $I.F.T.$ signify the forward and inverse Fourier transforms, respectively.

An alternative research approach to understand the role of vascular properties and wave reflection has been to model the cardiovascular system based on fundamental physical principles. If a model were developed that could also accurately predict pressure

and flow waveforms throughout the arterial network from noninvasively measured pressures, this would lend great clinical utility. The model predictions, if combined with information about cardiac output or stroke volume, could lead to estimates of cardiac systolic function (Kass, Maughan, Guo, Kono, Sunagawa, & Sagawa, 1987) and a better understanding of ventricular-vascular coupling (deTombe, Jones, Hunter, Burkhoff, & Kass, 1993). Since aortic systolic and diastolic pressures partially determine cardiac perfusion and loading, and aid in guiding pharmacological interventions in pathological conditions, the ability to accurately predict these pressures noninvasively is of significant interest. Accurately derived vascular properties from noninvasive measurements, as opposed to more difficult and riskier invasive measurements, would allow the study of large populations over time. Some vasoactive anti-hypertensive medications aim to increase artery compliance in vascular smooth muscle, and decrease arteriolar resistance (Cohn et al., 1995). Noninvasive measurement offers the potential to monitor the effectiveness of anti-hypertensive drugs by regularly gauging the vasculature of patients on these therapies.

The cardiovascular system is complex, and is difficult to model in three dimensions (Ottesen, Olufsen, & Larsen, 2004). Womersley (Womersley, 1957) developed mathematical models of pulsatile flow in elastic tubes. He assumed that the radial and azimuthal components of flow in vessels were small, thus reducing the problem from three dimensions to one dimension. He made further assumptions that allowed him to simplify the nonlinear equations to linear equations. The linear equations

were well suited for analysis in the frequency domain. These assumptions greatly reduce calculation complexity and make cardiovascular modeling feasible.

Note that both modeling approaches described above (the AR model and the Fourier analysis derived TF) apply a generalized TF to all patients and conditions. Our model is unique in that it produces vascular parameter estimates specific to the individual, yielding potentially valuable information about the patient's vasculature.

Specific Aim

The specific aim of this study is to predict blood pressure waveforms throughout the arterial network using noninvasive measurements and computational modeling.

Hypotheses

1. The model will be capable of predicting blood pressure waveforms at the femoral artery from radial artery recordings to within a root mean-squared error of 5 mmHg under varying hemodynamic conditions.

2. Changes in vascular properties induced by nitroglycerin and the cold pressor test will cause changes in estimated model parameters.

Chapter 2

MATHEMATICAL MODEL OF THE ARTERIAL CIRCULATION

Our model of the cardiovascular system is based on fundamental physical principles and anatomy. A nonlinear minimization algorithm in Matlab is used to analyze each perturbation in each individual by fitting the adjustable model parameters b_1, b_2 and a_{mult} (described below) to minimize the sum squared error between the measured and modeled waveforms at the femoral artery predicted from the radial artery (i.e. SSE_{min} of $SSE_{measured}$-$SSE_{modeled}$). Fitting is initiated from 27 different starting points (corresponding to all combinations (3x3x3) of high, medium, and low initial guesses for b1, b2, and a_{mult}) to ensure the true minimum is found in the allowed portion of 3D parameter space, in which the bounds are based on physiological limits. The overall best fit from the 27 starting points is the presumed global minimum error within the allowed parameter space, and the values of b1, b2, and a_{mult} from that best fit are saved for future analysis. The first version of the model was developed by Justin Spaeth and Dr. Antony Beris (Spaeth, 2006).

Anatomy

Figure 2.1 displays, to scale, the model's representation of the systemic circulatory network, consisting of 45 large tapered arteries of specified length and diameter (Ottesen, Olufsen, & Larsen, 2004).

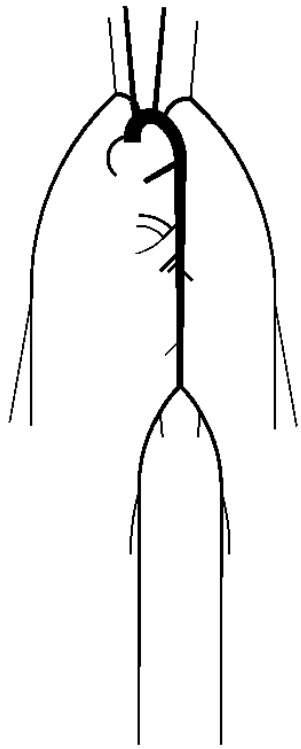

Fig. 2.1: Systemic Arterial Network **(Rose, WC; Johnson, DA; Spaeth, JR; Edwards, J; Beris, AN, 2008)**

Not shown in this figure, the 23 terminal large arteries have daughter branching capillary networks. Scaling laws specify the radii (r) and lengths (l) of these capillary networks (West, 1999). Vessels bifurcate (equations 2a and 2b) until their radius falls below 900 microns, then they trifurcate (equations 2c and 2d):

$$r_{n+1} = \frac{r_n}{\sqrt{2}} \tag{2a}$$

$$l_{n+1} = \frac{l_n}{\sqrt[3]{2}} \tag{2b}$$

$$r_{n+1} = \frac{r_n}{\sqrt[3]{3}} \tag{2c}$$

$$l_{n+1} = \frac{l_n}{\sqrt[3]{3}} \tag{2d}$$

where n and $n+1$ refer to the generation above and below the split, respectively. Once the radius of the following vessel generation is less than three microns (smaller than the size of a capillary), branching terminates. 18 to 21 generations comprise the daughter capillary networks; larger terminal arteries result in more daughter generations. In sum, 24 million vessels comprise the model, half of which lie at the final generation.

Wall Mechanics

Since the arterial walls are virtually incompressible (Carew, Vaishnav, & Patel, 1968), they are modeled as elastic tubes of finite thickness h, Young's modulus E_Y, and stiffness β:

$$\beta \equiv \frac{E_Y h}{\mathrm{r}} = b_1 \exp(-r/b_2) + b_3 \tag{3}$$

where b_1, b_2 and b_3 are constants (Ottesen, Olufsen, & Larsen, 2004). b_3 represents the large-vessel stiffness and has been set to $9\text{x}10^4$ Pa (see Figure 2.2), consistent with Ottesen, Olufsen, & Larsen, 2004. b_2 has units of length, and represents the radius at which the stiffness is the middle (in a logarithmic sense) of its transition from a stiff small-vessel value ($\beta = b_1 + b_3$ when r=0, where $b_1 + b_3$ represents small-vessel stiffness) to a less-stiff large-vessel value ($\beta = b_3$ when r is large). The dependence of stiffness (β) on diameter (r) is shown in Figure 2.2.

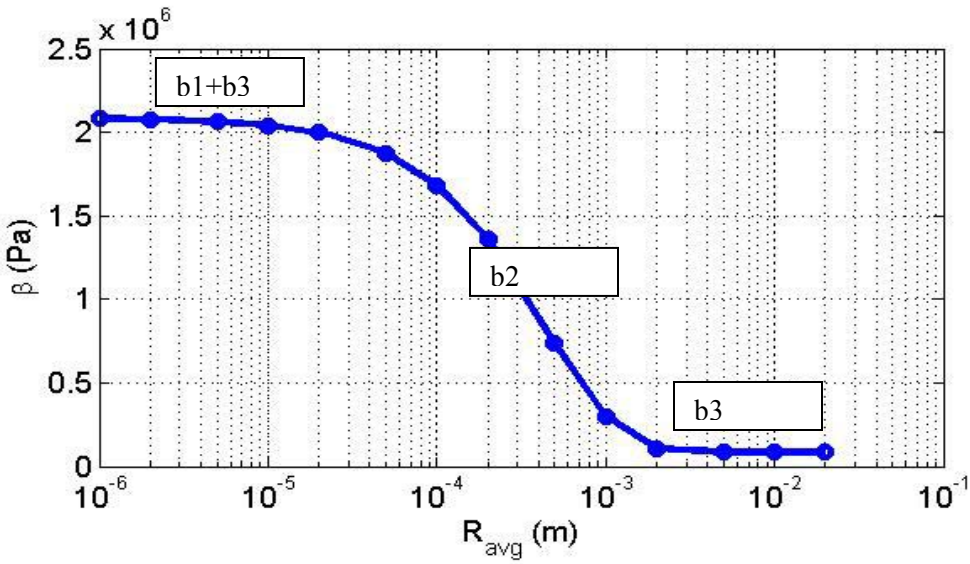

Fig. 2.2: β vs r (Rose, WC; Johnson, DA; Spaeth, JR; Edwards, J; Beris, AN, 2008)

Small Diameter Adjustment

Model parameter a_{mult} is introduced to allow for variability and adjustment of small vessel diameter. Without a_{mult}, all of the vessel diameters would be fixed by equations 2a and 2c. Thus small vessel diameter would be entirely dependent on parent vessel diameter, but not adjustable. Since fixation of vascular diameters results in an inability to adjust total peripheral resistance, model parameter a_{mult} alleviates this concern. Diameter adjustment is implemented so that capillary diameter is constant (since capillaries lack smooth muscle and their diameters are presumed not to be subject to physiological control) and so that daughter vessels are always narrower than the parent vessel, even after adjustment. An equation was developed to implement such diameter control in the generated arterial trees. The results are displayed in Figure 2.3 below,

which shows vessel diameter as a function of arterial tree generation number (where 1 corresponds to the largest artery in a daughter branching capillary network and 20 corresponds to a capillary) at varying values of a_{mult} [a_{mult}=0 (i.e. unadjusted), a_{mult}=2 (larger diameters), and a_{mult}=-0.85 (smaller diameters)]. Changes in a_{mult} affect TPR and may affect wave reflection, since vessel impedance is a function of diameter, as well as other factors.

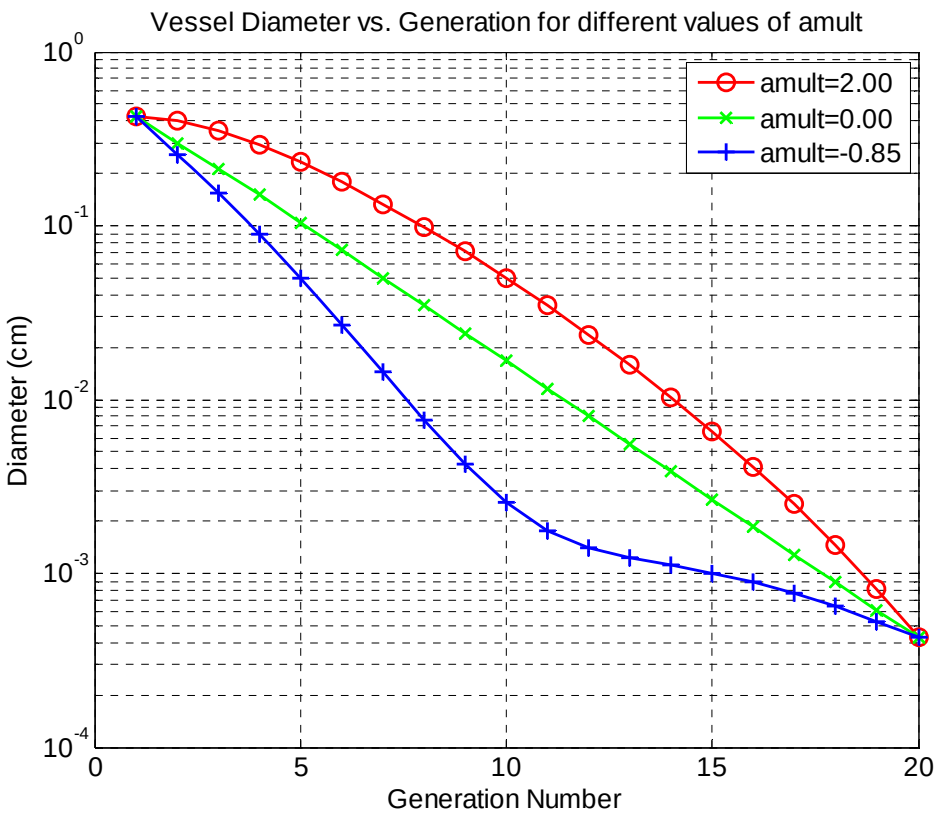

Figure 2.3

Chapter 3

RESEARCH DESIGN AND METHODS

Healthy adults were recruited and screened to ensure that they were adequately healthy to participate in the study. Continuous blood pressure was measured under different conditions (baseline, cold pressor test, nitroglycerin) using applanation tonometry at the carotid, radial, and femoral arteries. The availability of multiple sites allowed for prediction and comparison of modeled pressure waveforms with experimentally recorded waveforms.

Subjects

Apparently healthy adults (men and women) between the ages of 20 and 35, inclusive, were recruited for the study, which involved one 3.5 hour visit. Subjects were provided an informed consent for review prior to the screening. Prior to arrival, subjects were encouraged to be sufficiently hydrated, and to refrain from alcohol, caffeine, and exercise for at least 12 hours before the visit. Upon arrival at the Human Performance Lab, subjects received a description of the experiment and potential risks and benefits, and then provided informed consent.

Screening

Subjects were screened at the Human Performance Lab (in the Vascular Physiology Lab) to ensure that they were adequately healthy to complete the experimental protocol. First, subjects completed a medical history questionnaire. Next,

the following information was obtained: age, blood pressure (seated and standing), height, weight, hematocrit, and hemoglobin content (via collection of a blood sample from a finger prick). Note that the hematocrit value represents the fraction of red blood cells, and the hemoglobin value represents the quantity of oxygen-transport protein in the blood. Finally, women completed a pregnancy test.

Exclusion criteria included any of the following: a medical history concern (to be determined by the principal investigator), smoking, recent use of nitrate drugs, an age less than 20 or greater than 35, a systolic blood pressure greater than 139 or less than 100, a diastolic blood pressure greater than 89, a weight less than 100 lbs, a body-mass index of greater than 30 kg/m^2, a hematocrit value greater than 49% (46% females) or less than 37% (36% females), a hemoglobin value greater than 18 g/dl (16 g/dl females) or less than 13 g/dl (12 g/dl females), or a positive pregnancy test result.

Cardiac Output and Flow Measurement

In order to estimate the blood volume pumped by the subject's heart per minute, a cardiac output test was performed. This estimate was to be compared with the cardiac output predicted by the model.

In this procedure, first a heart rate monitor was attached around the subject's chest, and the subject was asked to breathe room air comfortably through a mouthpiece. Once the tidal volume stabilized, the subject breathed into and out of a bag of a known volume and carbon dioxide and oxygen concentration for 15 seconds. This protocol was

repeated approximately five times for each subject. By measuring the expired carbon dioxide and oxygen concentration, an estimate of cardiac output was obtained.

Because our model provides flow predictions, flow measurements were experimentally collected for comparison. Ultrasound imaging was applied to the radial, brachial, carotid, and femoral arteries to generate artery diameter estimates (from which an artery area was derived). Next, a Doppler probe was applied to the same recording artery sites to generate blood velocity estimates. By combining the diameter and velocity estimates, flow measurements were collected and averaged to obtain a single flow waveform over one cardiac cycle.

Blood Pressure Measurement

First, three adhesive electrodes were affixed to the subject's chest in order to capture the electrocardiogram (ECG). Next, the subject lay supine for ten minutes to allow blood pressure to stabilize. Multiple brachial cuff systolic and diastolic blood pressures were taken via the technique of oscillometric sphygmomanometry. To generate the pressure waveform estimates, the technique of applanation tonometry was used. At the radial and femoral arteries in all subjects (and the carotid artery in some subjects), a high-fidelity pointed strain gauge transducer (Millar Instruments) about the size of a pencil was applied to the artery site of interest and clamped, and a pressure recording was captured using a custom-developed Labview data acquisition program. Stable pressure records of at least ten seconds duration were divided into beats by means of the R waves of the ECG, which was also recorded. Each beat was adjusted to have a duration equal to the average beat duration, and then the beats were averaged to estimate the average single

beat pressure waveform in that artery, beginning at the R wave of the ECG. The brachial cuff pressure measurements were used to calibrate the tonometer waveforms, as follows. The mean cuff pressure (1/3 systolic + 2/3 diastolic) was set equal to the average voltage of the tonometer waveform, and the diastolic cuff pressure was set equal to the minimum voltage from the tonometer waveform.

Repeat with foot in cold water: After collection of baseline data, the subject was asked to place his or her bare foot in a container of cold water (35-40°F) at the end of the table. This perturbation caused an increase in blood pressure via sympathetic vasoconstriction of the arteries. Brachial cuff systolic and diastolic blood pressures were taken at two and ten minutes. Applanation tonometry was repeated at the different artery sites of measurement.

Repeat with nitroglycerin administration: Following a fifteen minute rest period, the subject placed a small tablet of 0.3 mg nitroglycerin (NTG) under the tongue to be dissolved. This caused a modest decrease in blood pressure via vasodilation of the arteries (hence NTG is used to treat angina pectoris by dilating and thus enhancing blood flow through the coronary arteries). Brachial cuff systolic and diastolic blood pressures were taken at two and ten minutes. Applanation tonometry was repeated at the artery sites of measurement. Next, the distance between the measurement sites was measured. Before discharging the subject, their blood pressure was checked to ensure that it had returned to baseline values.

Statistical Analysis

Differences in mean values of fitted model parameters between conditions were tested with single factor analysis of variance. If warranted (by a significant F statistic in the ANOVA), Tukey tests were used to determine which pairs of conditions had different means. A probability of $p<0.05$ was considered significant.

Chapter 4

RESULTS

Experimental Tonometry Recordings

Figure 4.1, below, shows a representative sample of calibrated tonometry recordings at the radial, femoral, and carotid artery sites. Much information about the arterial vasculature may be derived from such recordings. First, consider the increase in systolic pressure at increasing distances away from the aortic root. Wave reflection is the phenomenon responsible for this pulse pressure amplification, and arises when some of the pressure and flow of the forward-ejected blood is reflected back towards the heart. Arterial branching patterns and resistance vessels comprise the main reflection sources. Next, observe the lag in the timing of the upstroke of the femoral and radial artery recordings relative to the carotid recording. Quantification of this lag, combined with a measurement of the distance between the corresponding recording sites, allows for determination of the speed of the wave propagated from the heart, termed the pulse wave velocity (PWV). PWV is a clinically valuable index; stiffer arteries produce higher PWVs. Finally, note the irregular femoral recording shape. This demonstrates the sensitivity of the technique of applanation tonometry. Particular attention should be paid to applanation pressure, angle, and positioning on the artery.

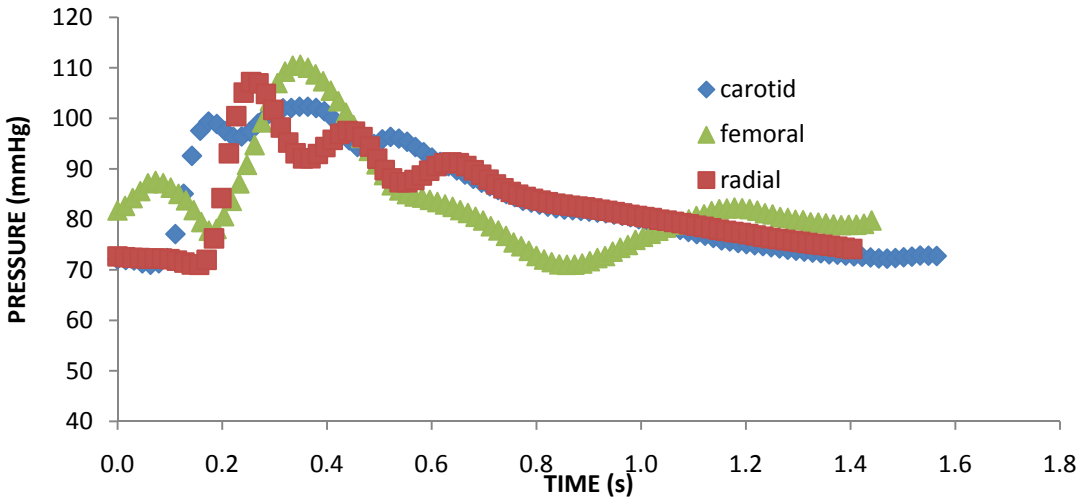

Fig. 4.1: Representative Calibrated Tonometry Recordings

Several experimental measurement techniques yielded inconsistent data. First, the cardiac output (CO) data in early subjects was highly variable, thus this measurement was not conducted in all subjects, and was not compared to the CO model predictions. Similarly, ultrasonic velocity and diameter measurements of high quality were not always obtainable in all vessels under all conditions. We wished to perform the same data analysis procedures on the data from all subjects under all conditions. Therefore, the cardiac output and ultrasonic velocity and diameter data, which was unavailable in some subjects, was not used for model identification purposes.

Figures 4.2 through 4.23, on the following pages, show the calibrated, experimental tonometry recordings collected at the radial and femoral artery sites. Carotid pressure recordings were not used in the final parameter estimation, due to their greater variability, as will be discussed further in the Statistical Analysis section below. Therefore the carotid pressure recordings are not shown in these figures.

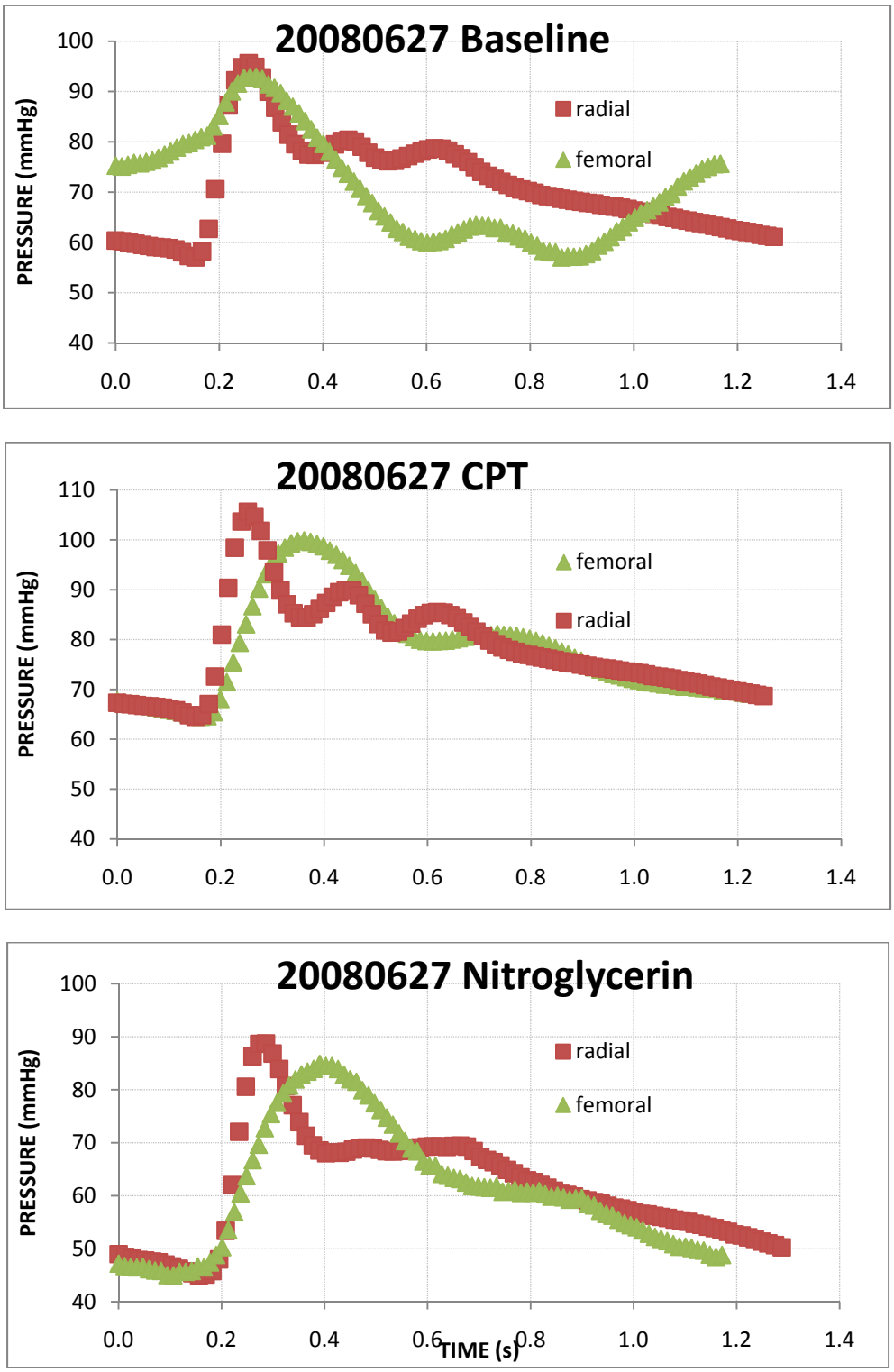

Fig. 4.2: 20080627 Experimental Tonometry Recordings

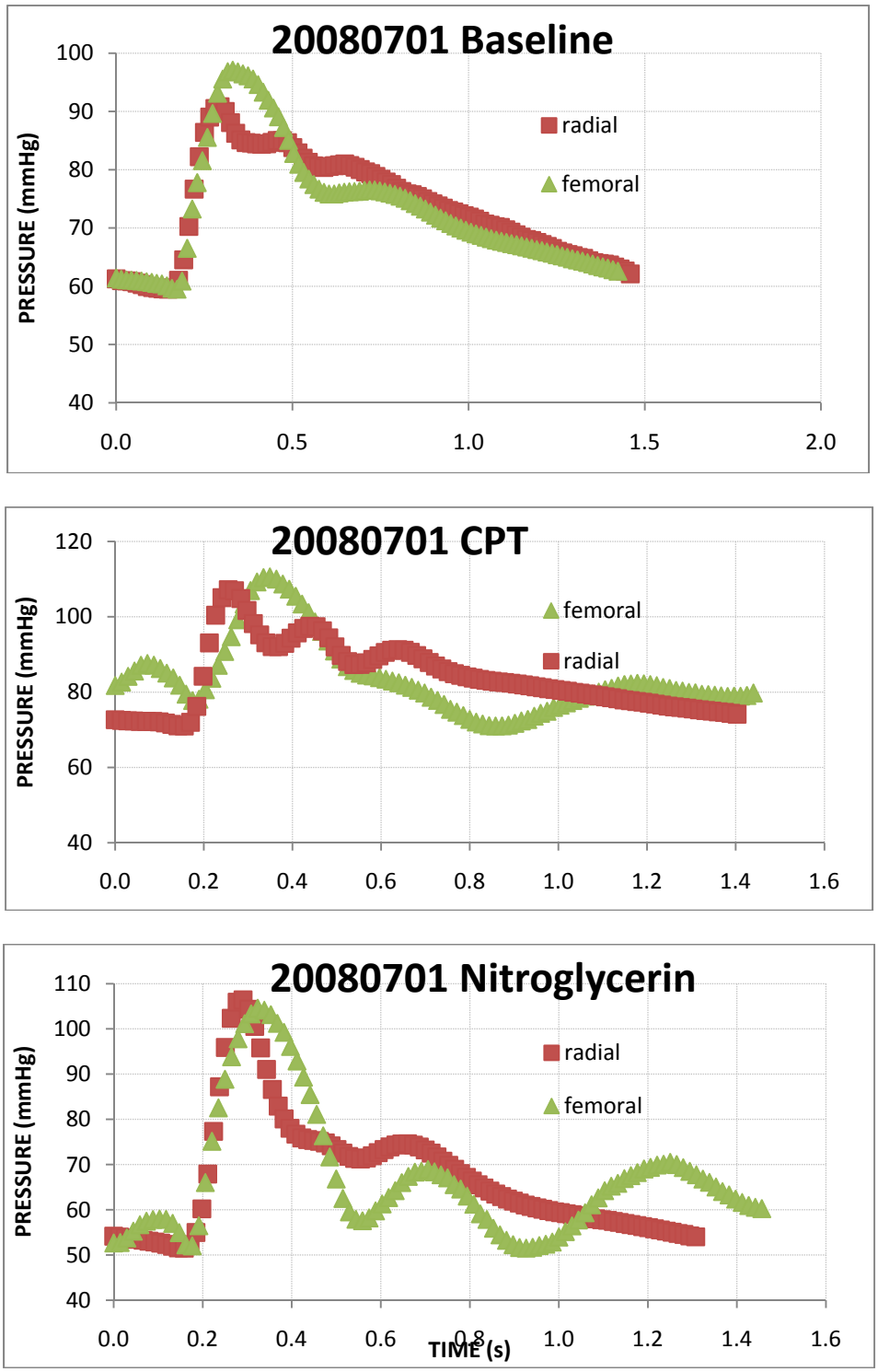

Fig. 4.3: 20080701 Experimental Tonometry Recordings

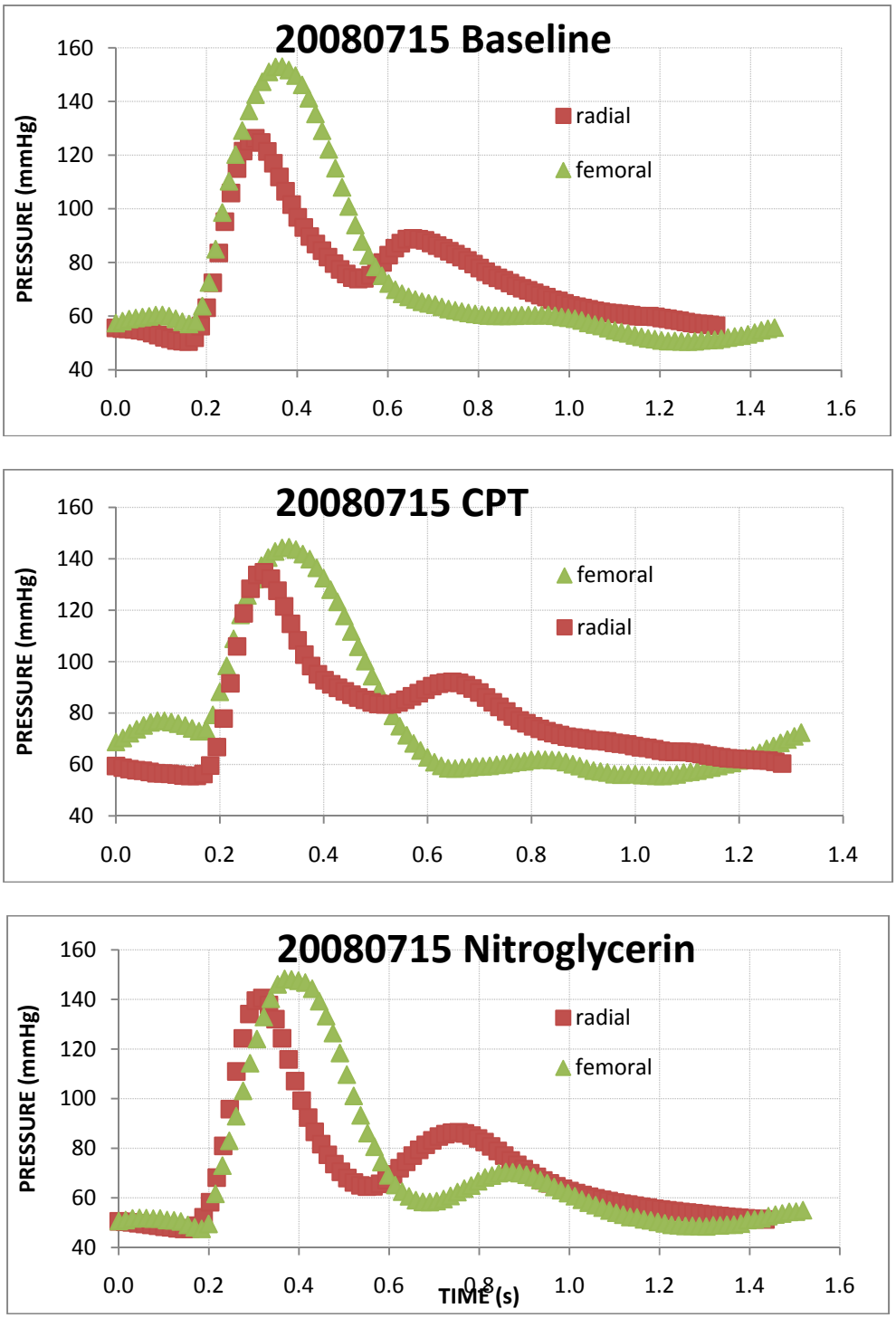

Fig. 4.5: 20080715 Experimental Tonometry Recordings

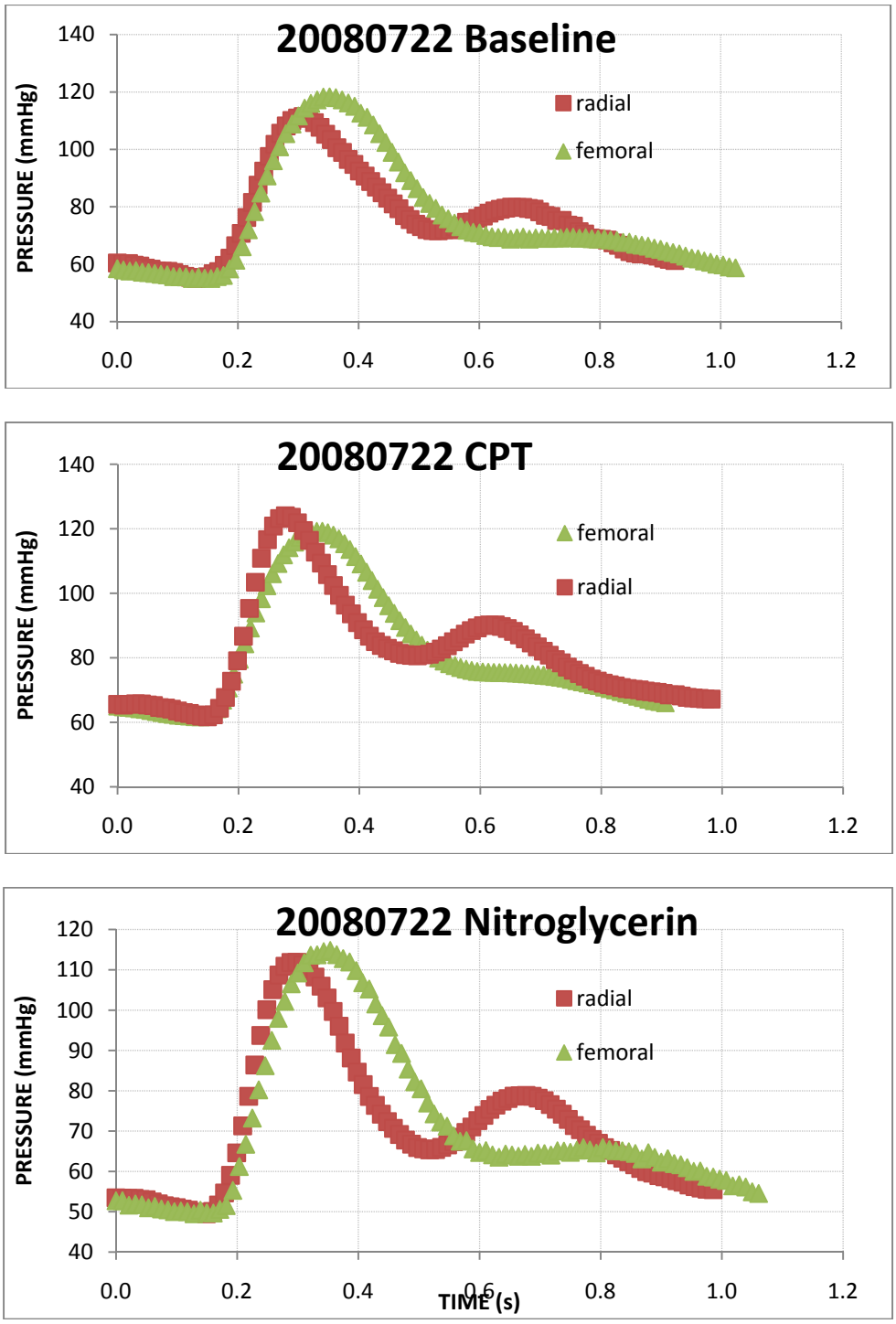

Fig. 4.6: 20080722 Experimental Tonometry Recordings

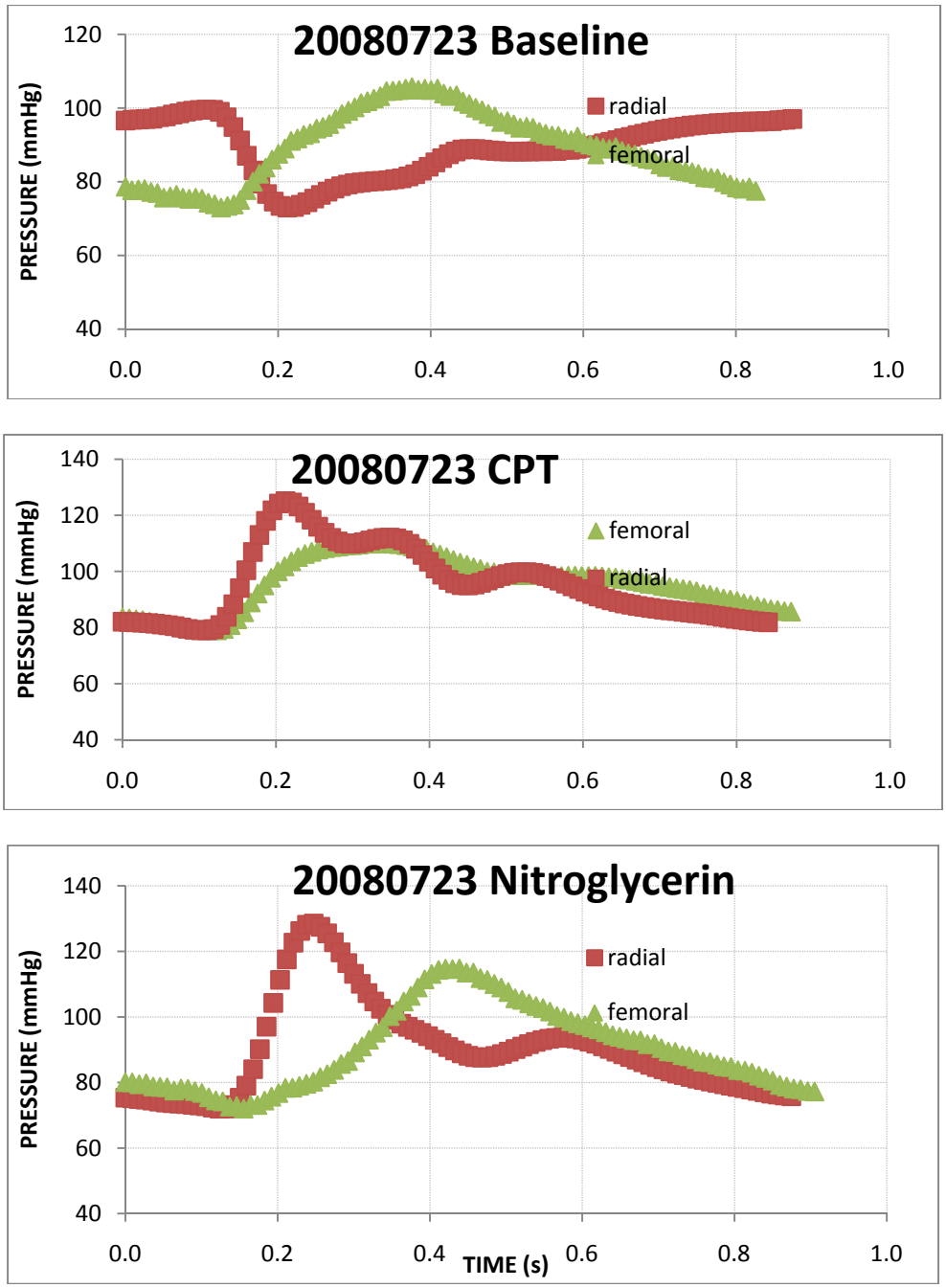

Fig. 4.7: 20080723 Experimental Tonometry Recordings

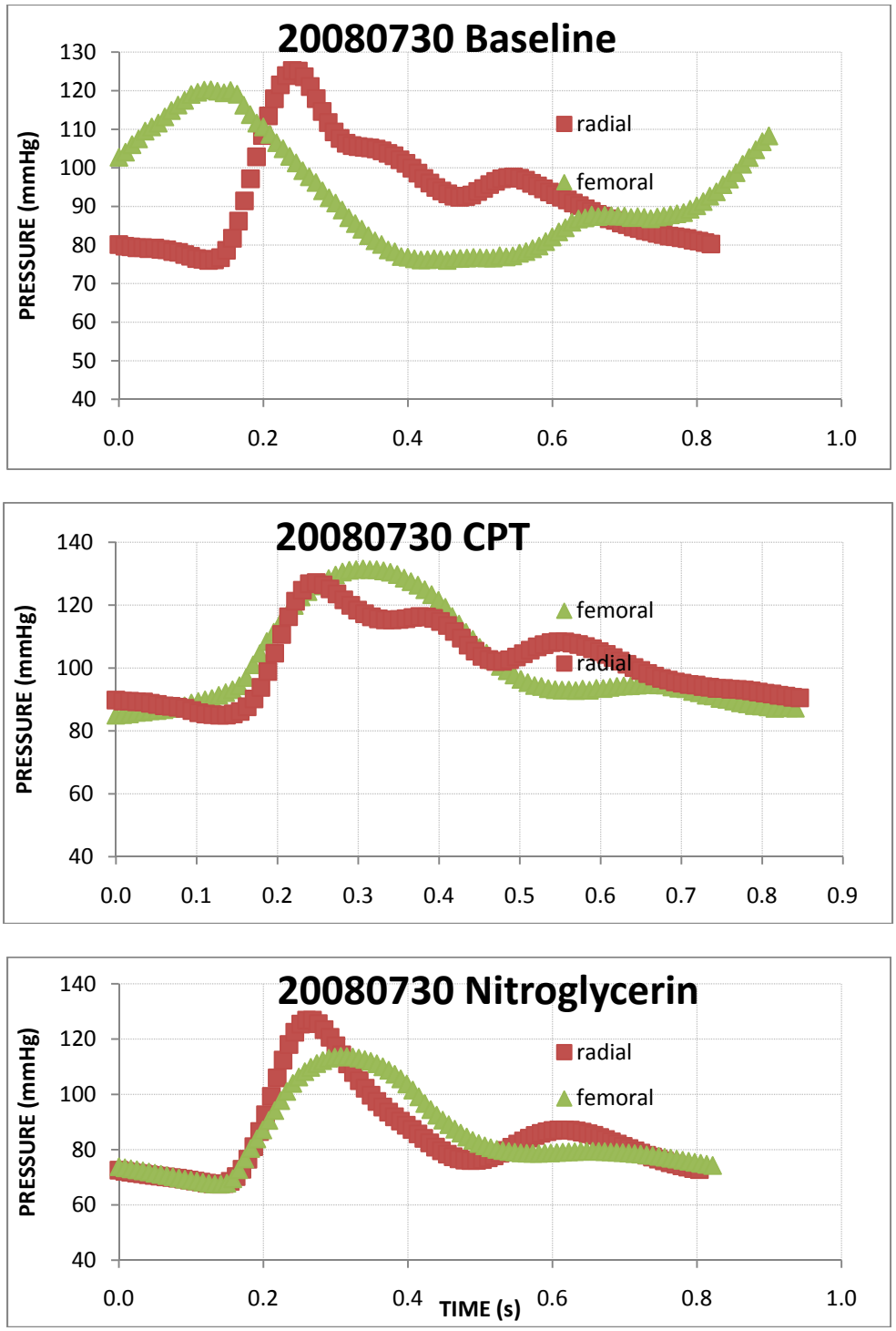

Fig. 4.8: 20080730 Experimental Tonometry Recordings

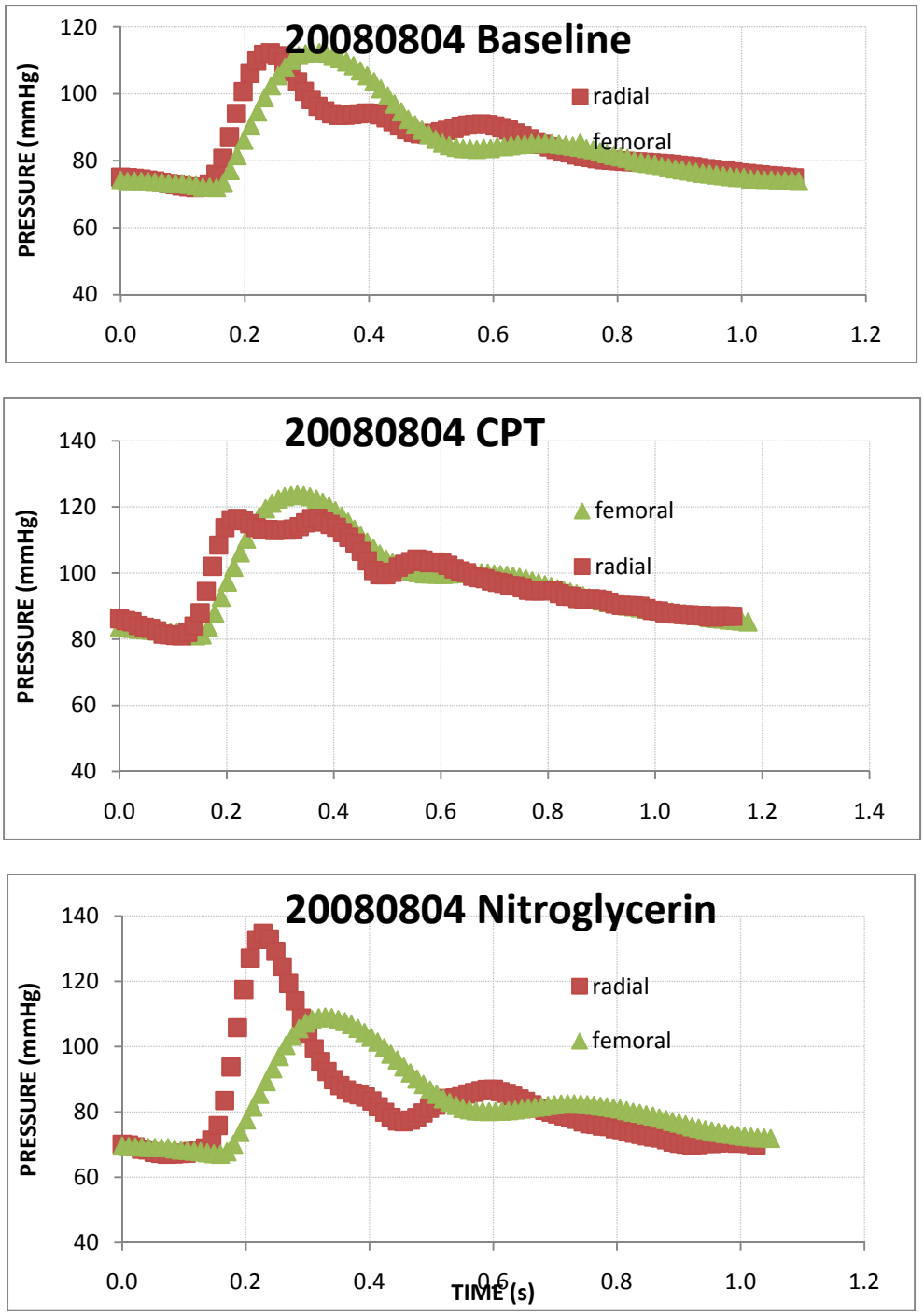

Fig. 4.9: 20080804 Experimental Tonometry Recordings

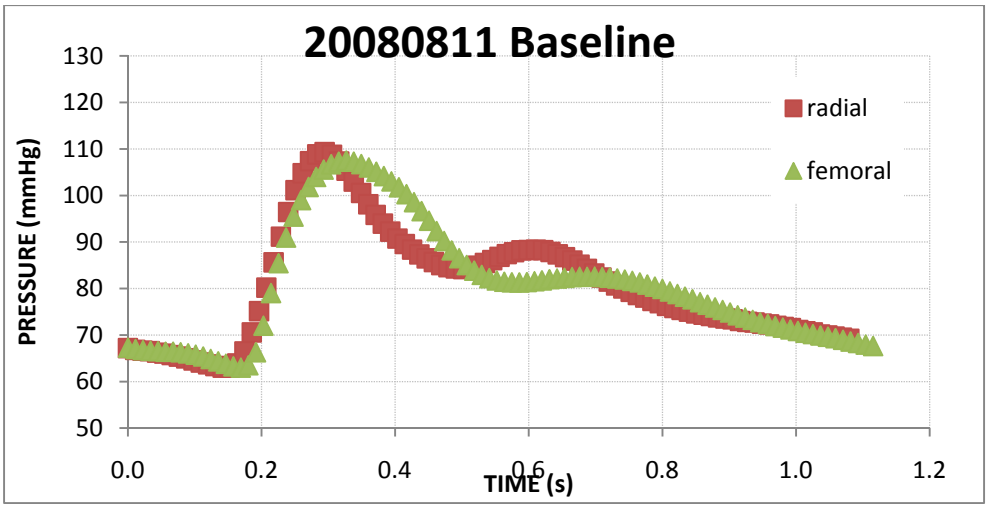

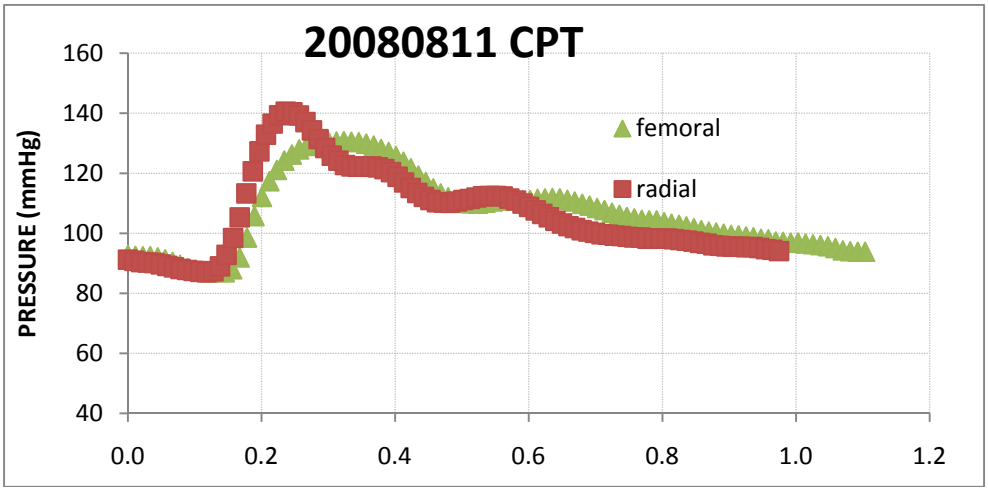

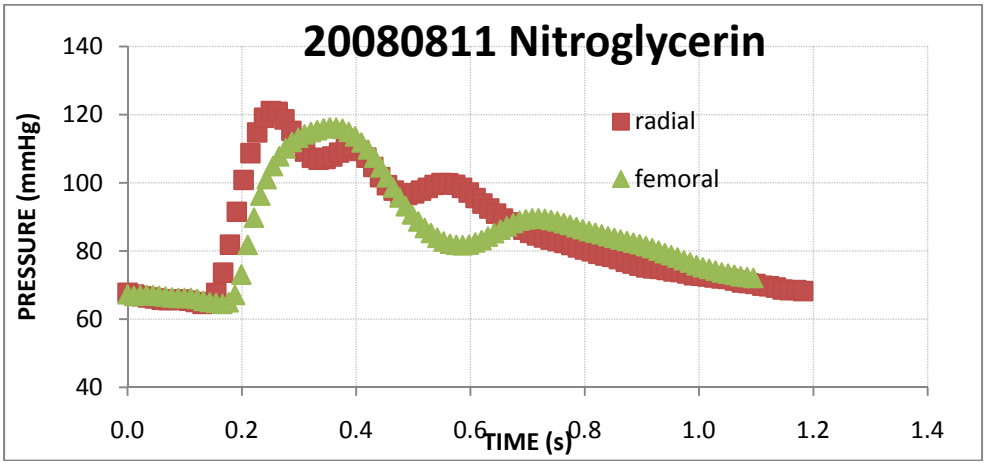

Fig. 4.10: 20080811 Experimental Tonometry Recordings

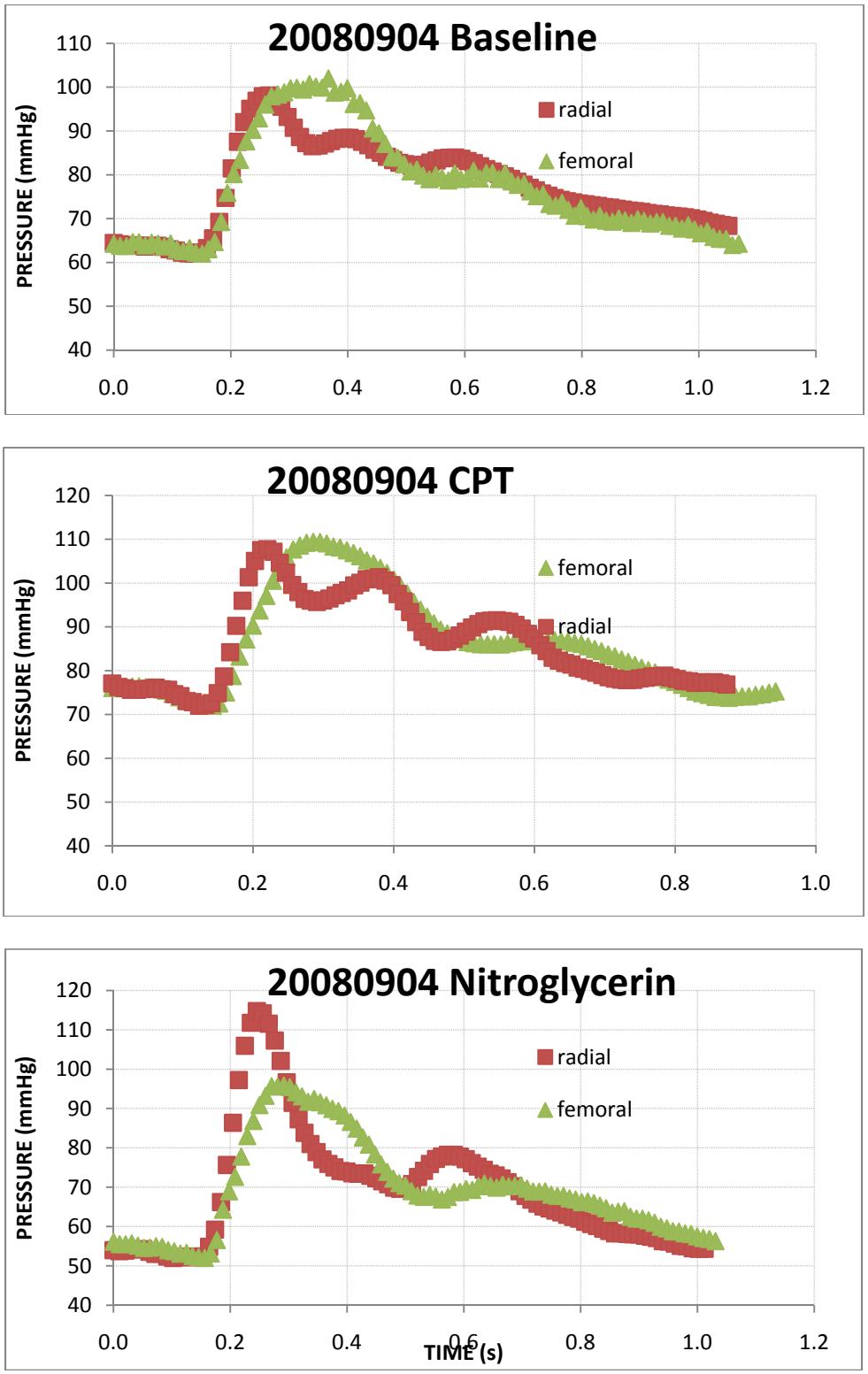

Fig. 4.11: 20080904 Experimental Tonometry Recordings

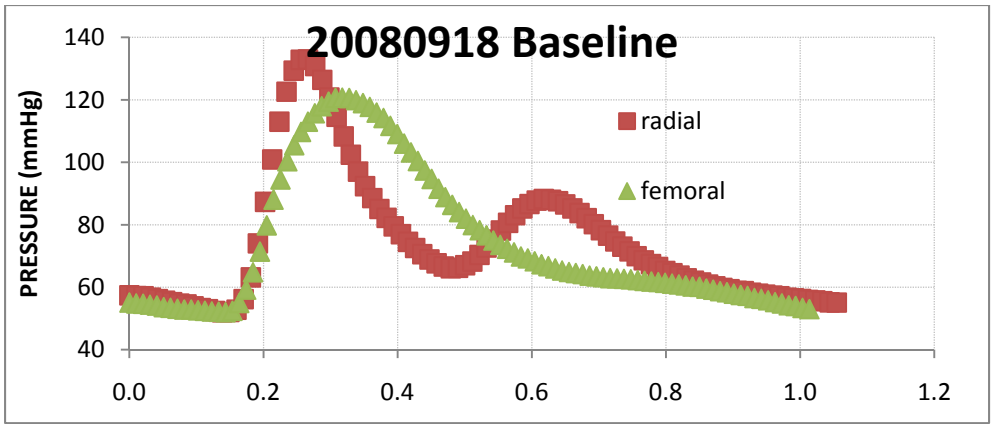

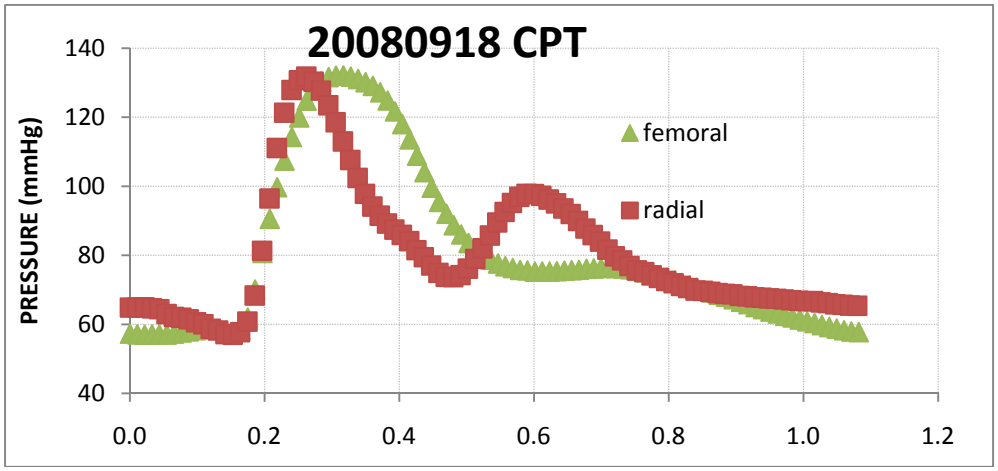

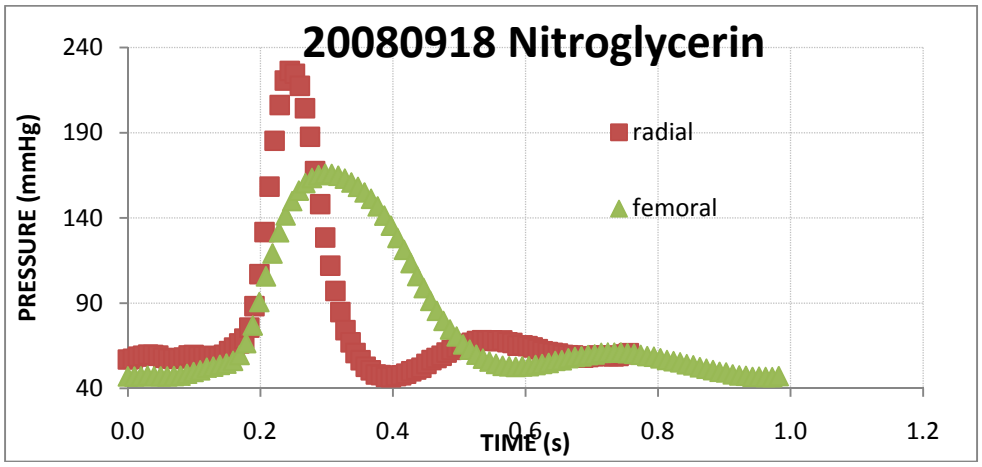

Fig. 4.12: 20080918 Experimental Tonometry Recordings

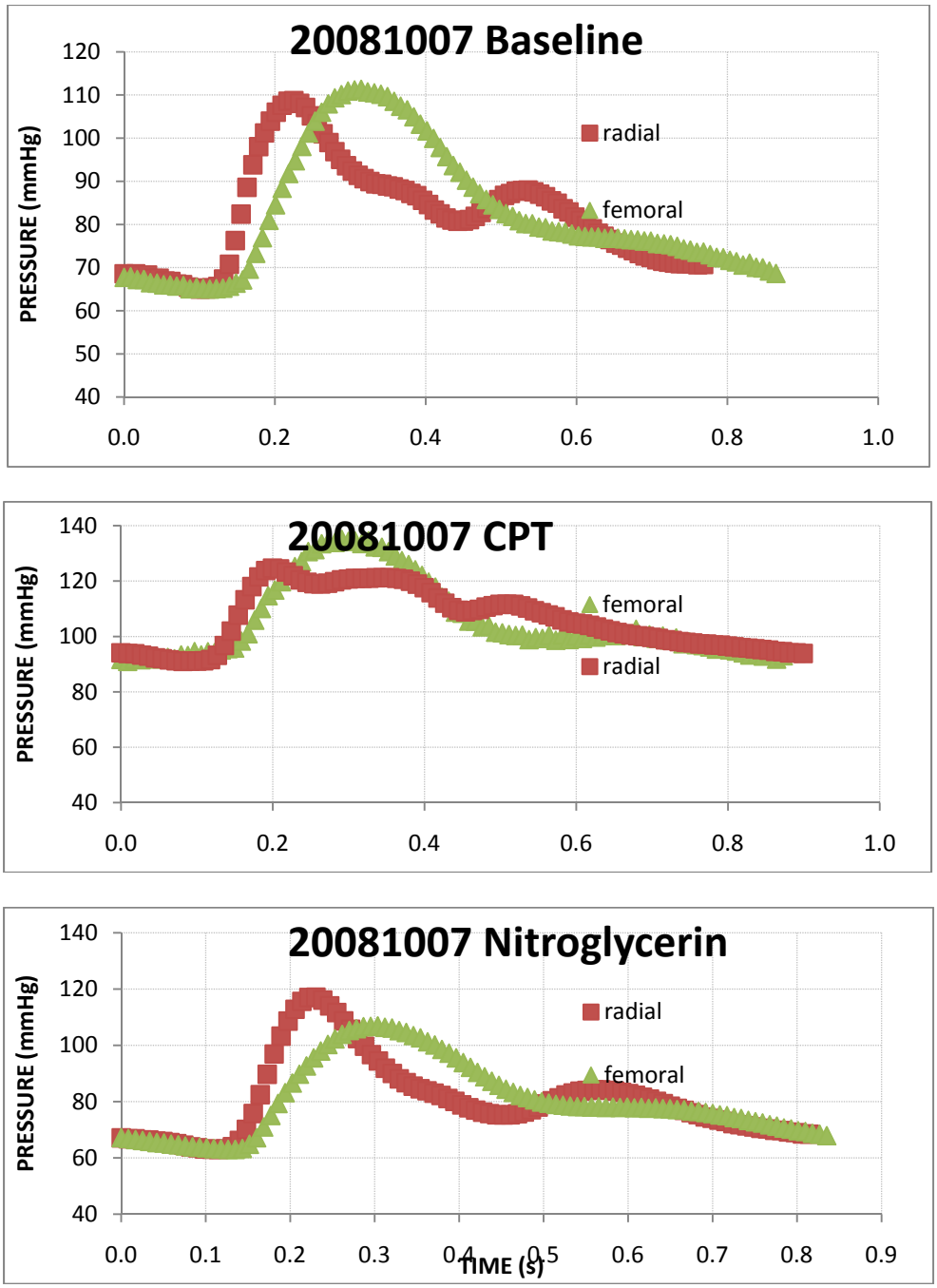

Fig. 4.13: 20081007 Experimental Tonometry Recordings

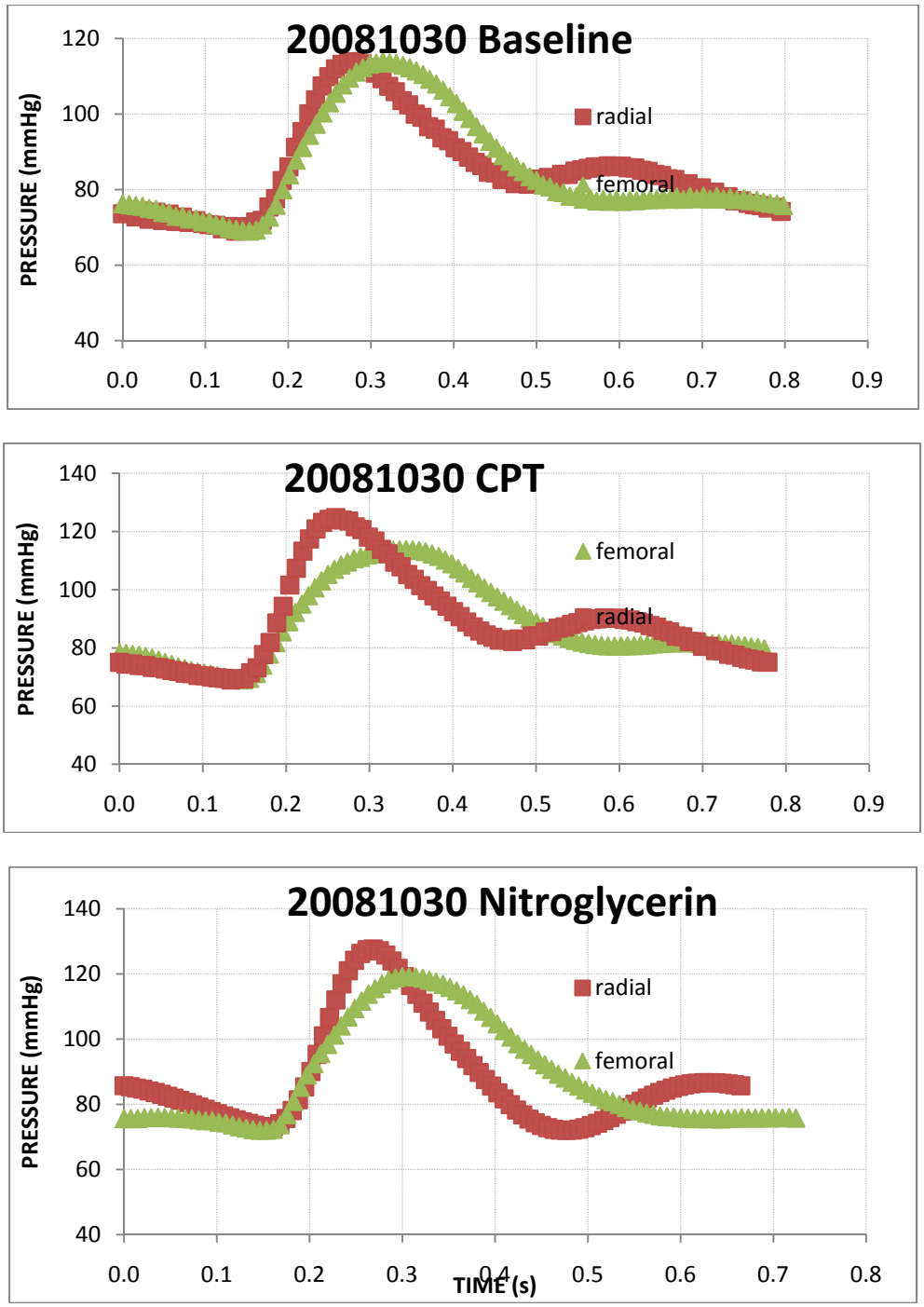

Fig. 4.14: 20081030 Experimental Tonometry Recordings

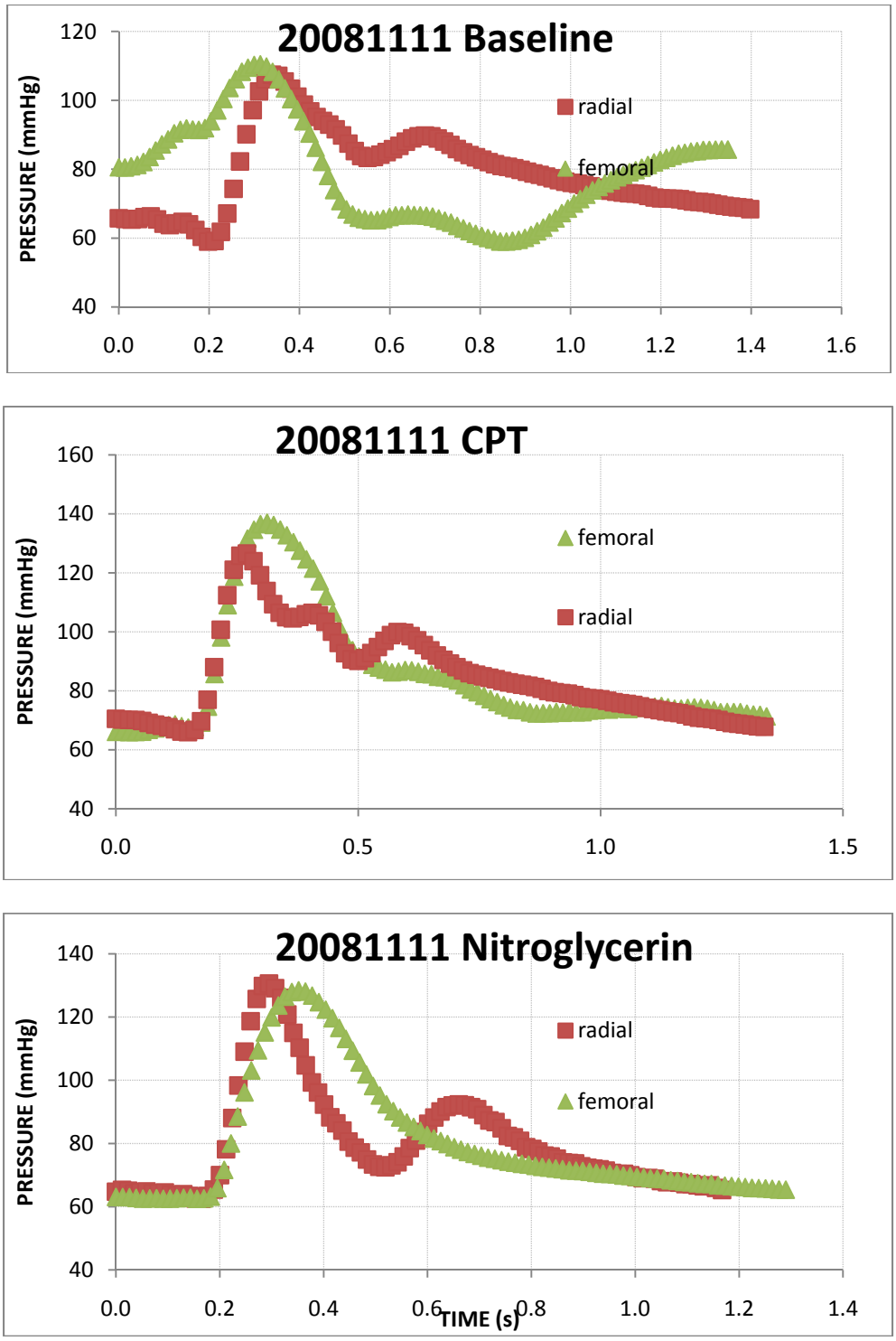

Fig. 4.15: 20081111 Experimental Tonometry Recordings

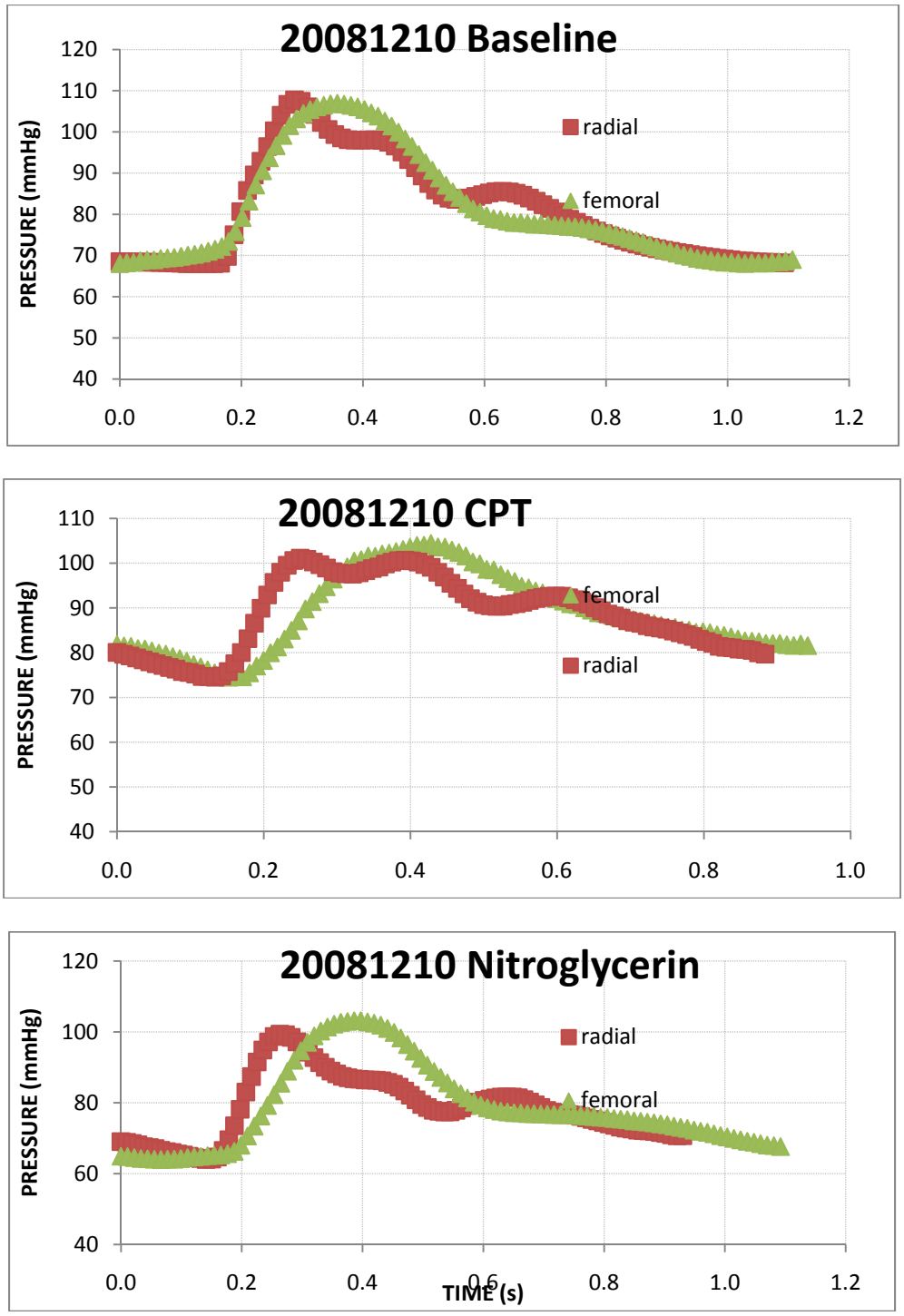

Fig. 4.16: 20081210 Experimental Tonometry Recordings

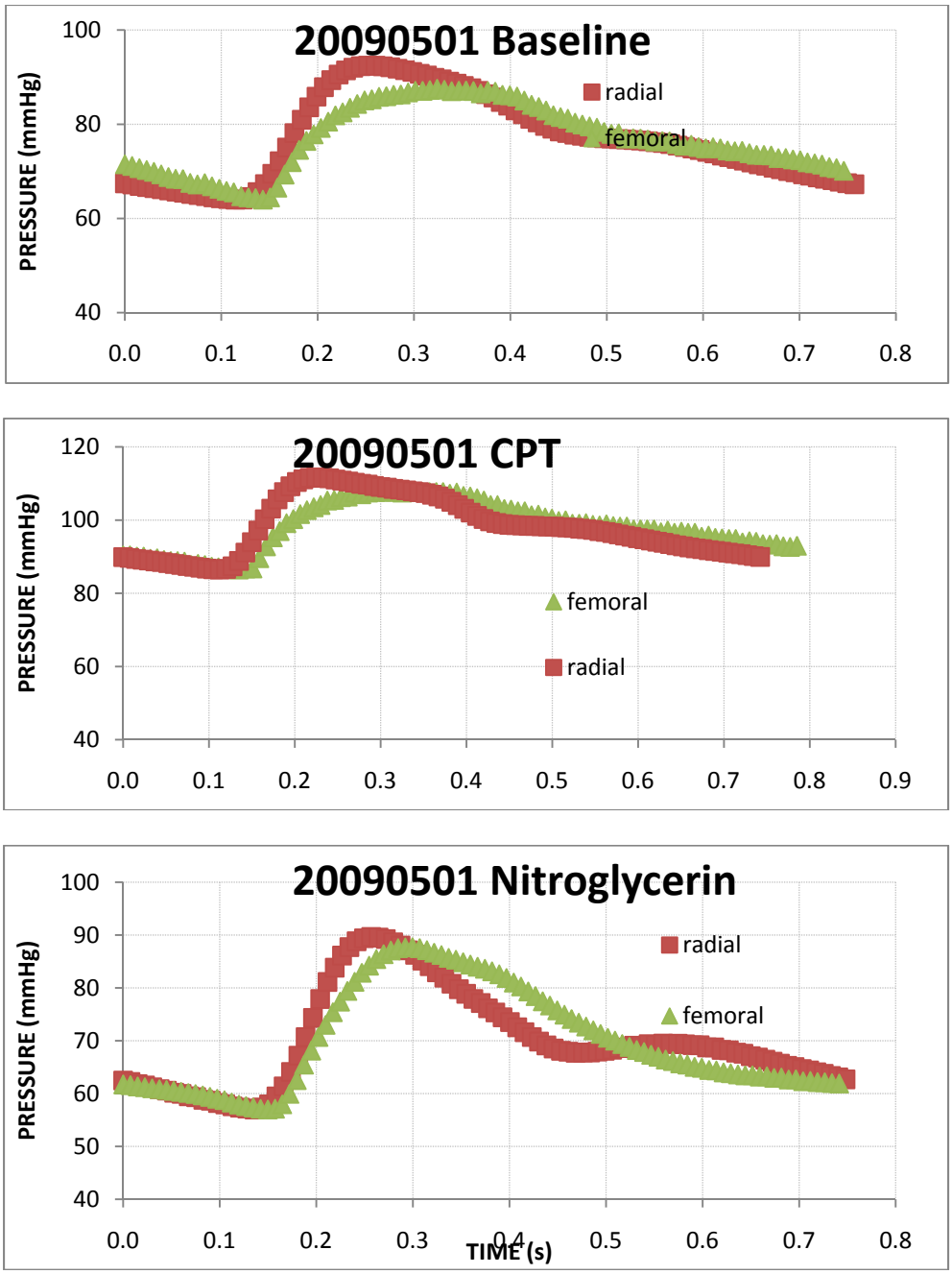

Fig. 4.17: 20090501 Experimental Tonometry Recordings

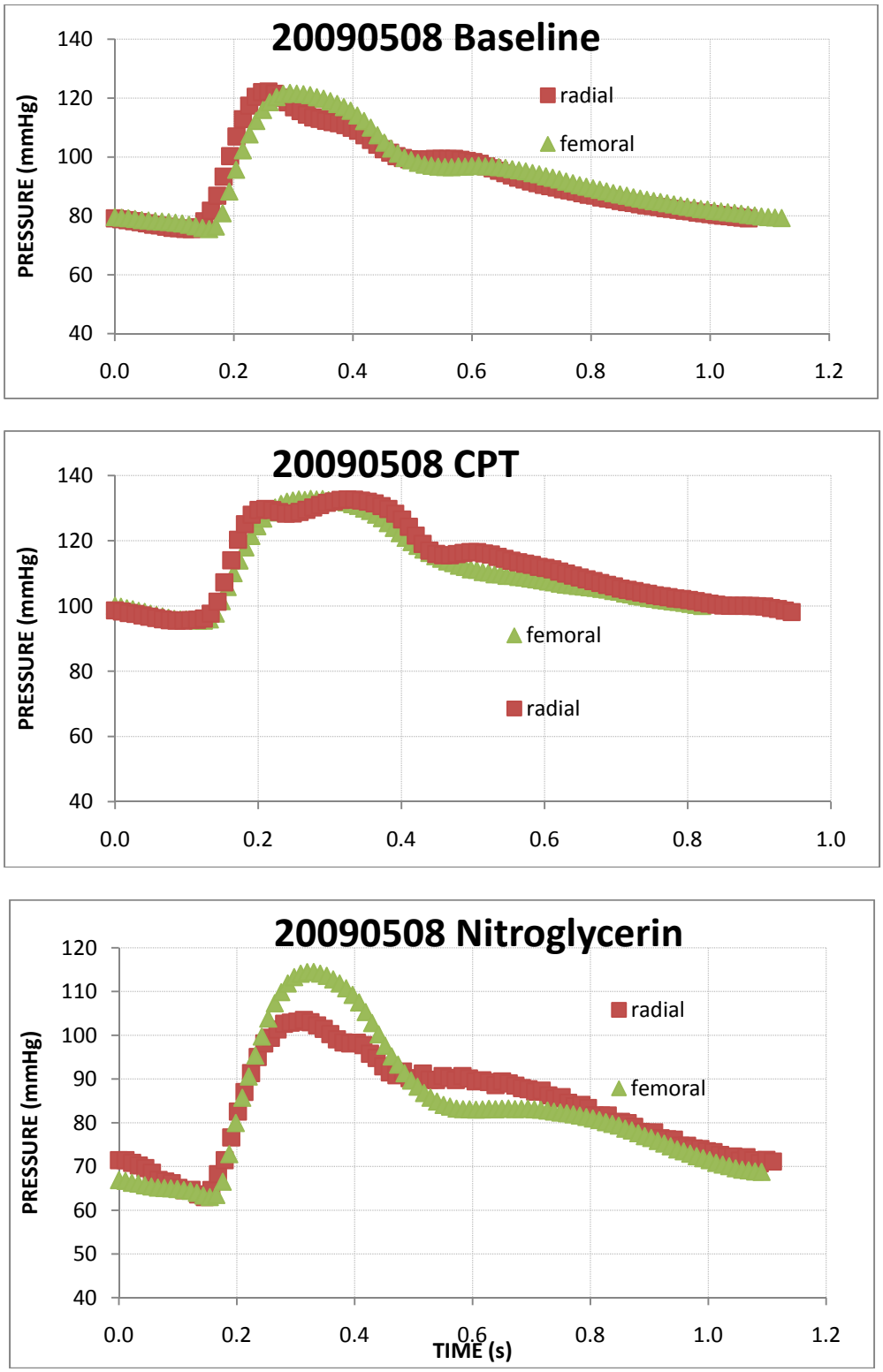

Fig. 4.18: 20090508 Experimental Tonometry Recordings

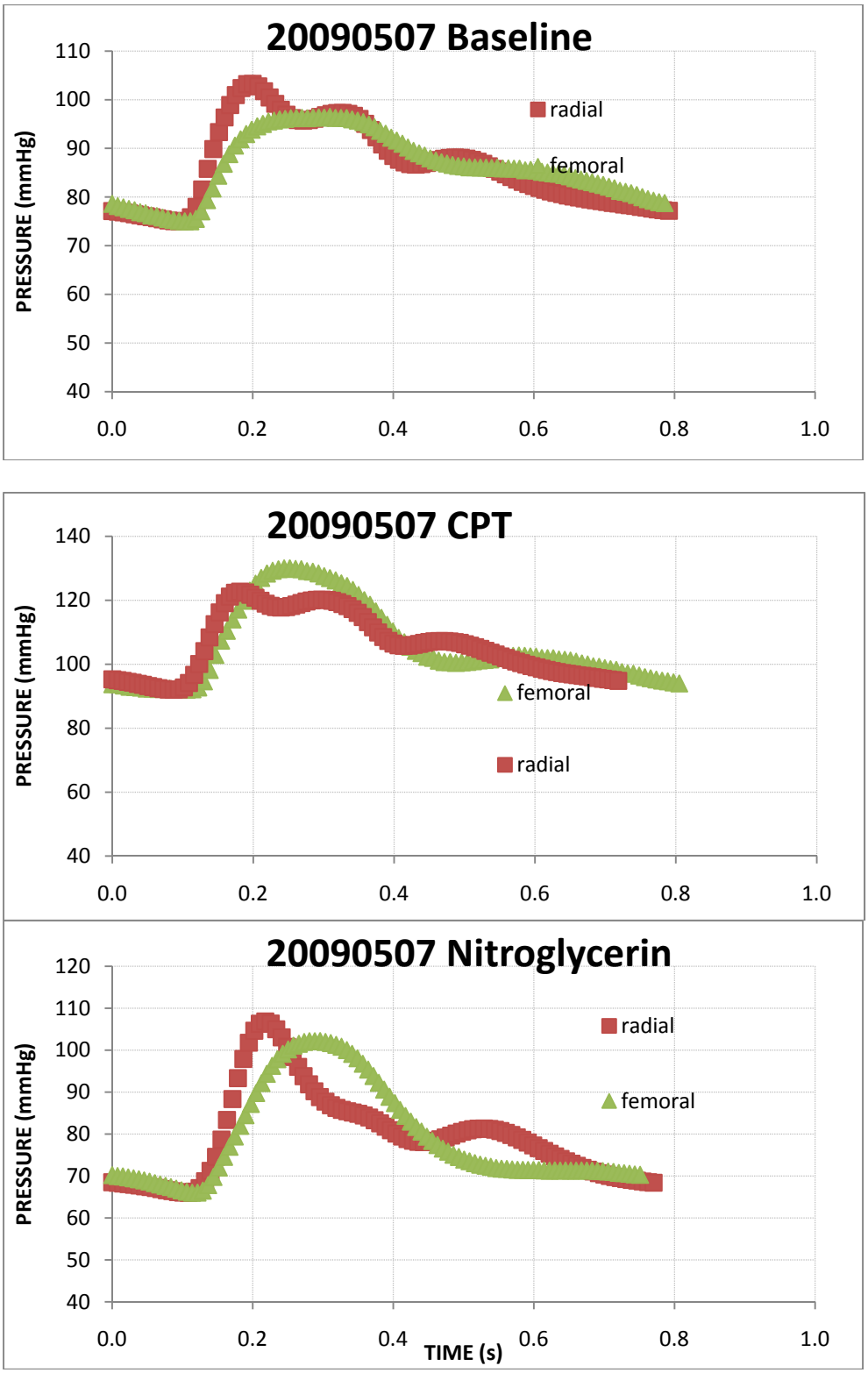

Fig. 4.19: 20090507 Experimental Tonometry Recordings

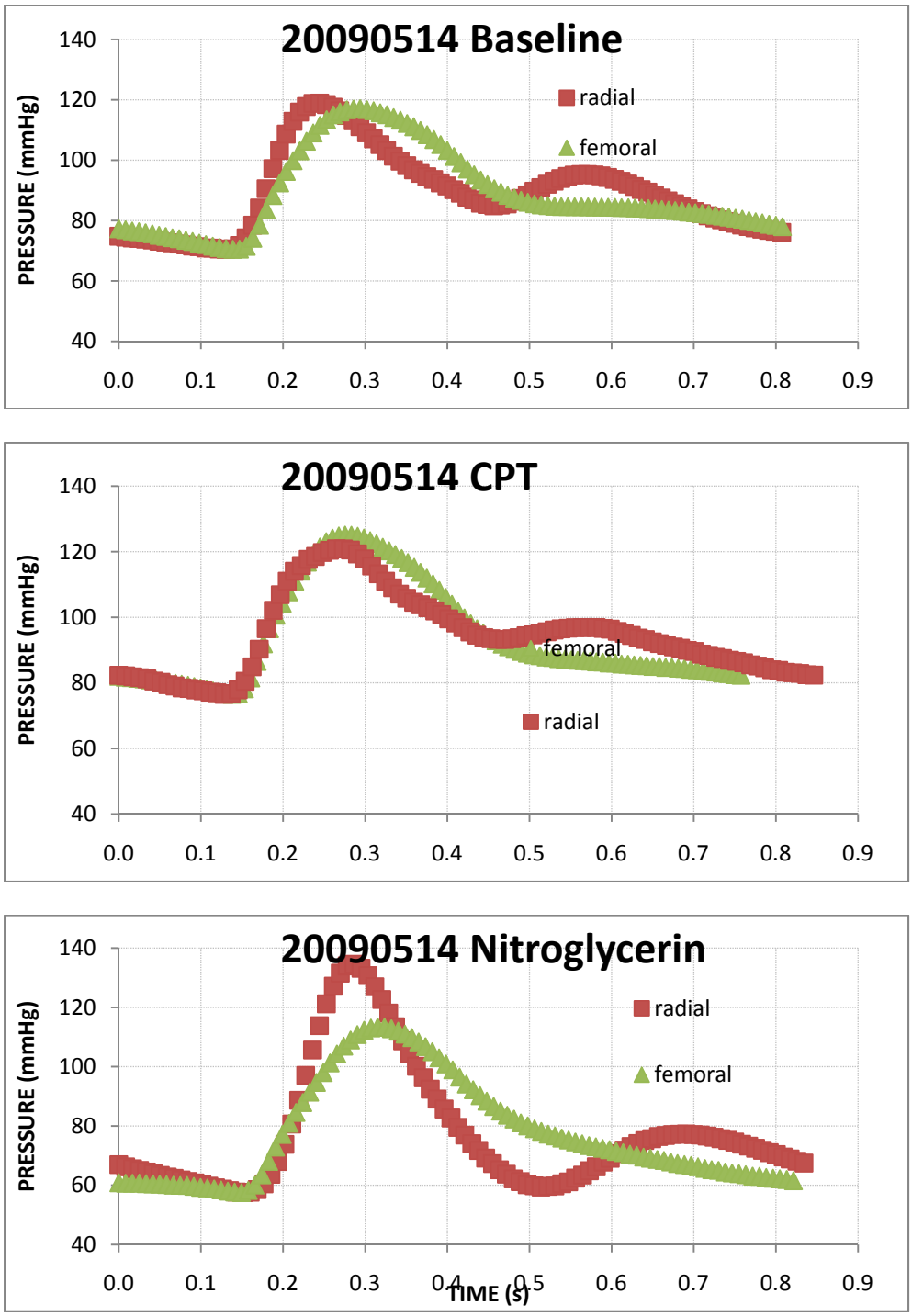

Fig. 4.20: 20090514 Experimental Tonometry Recordings

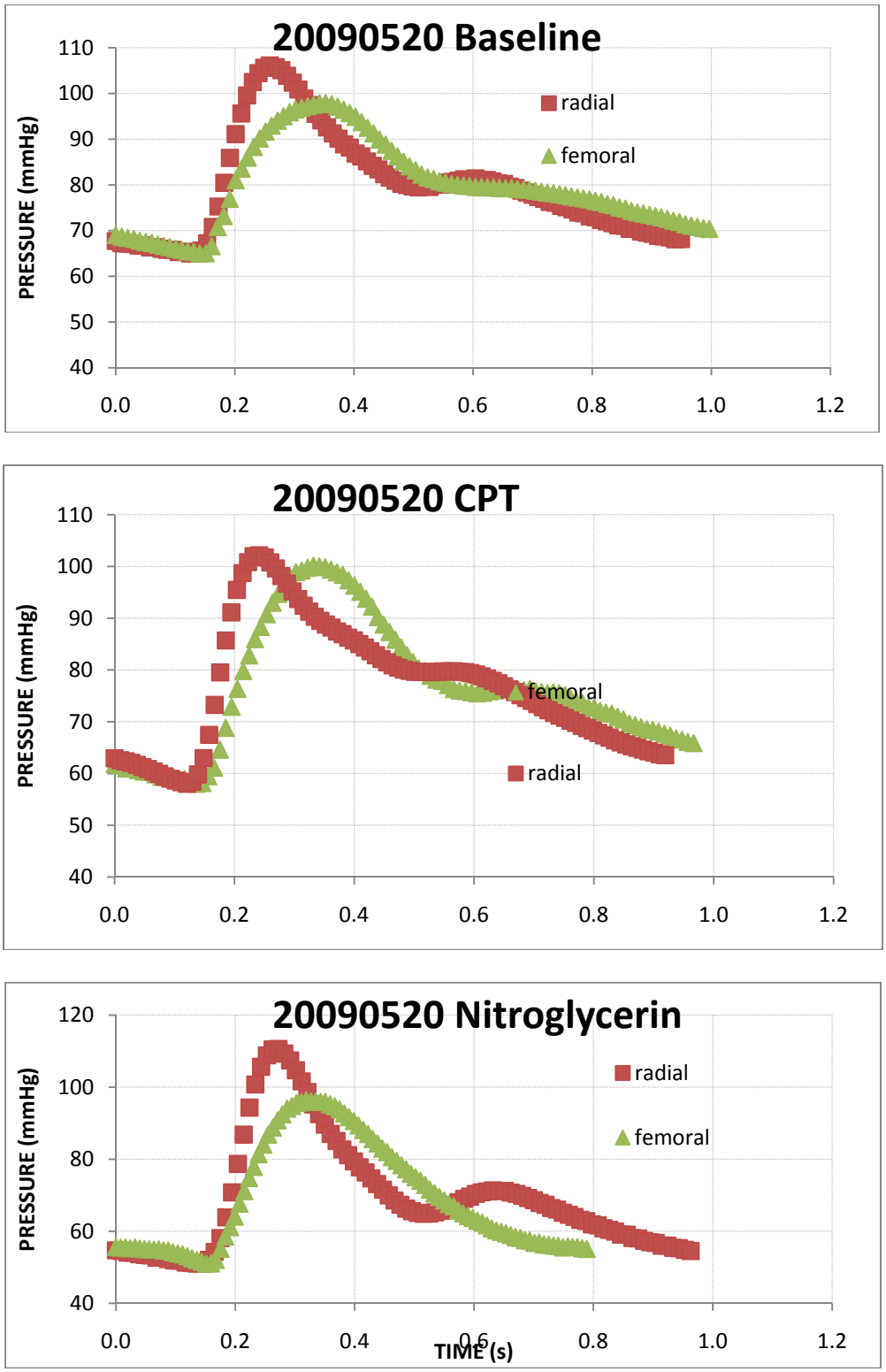

Fig. 4.21: 20090520 Experimental Tonometry Recordings

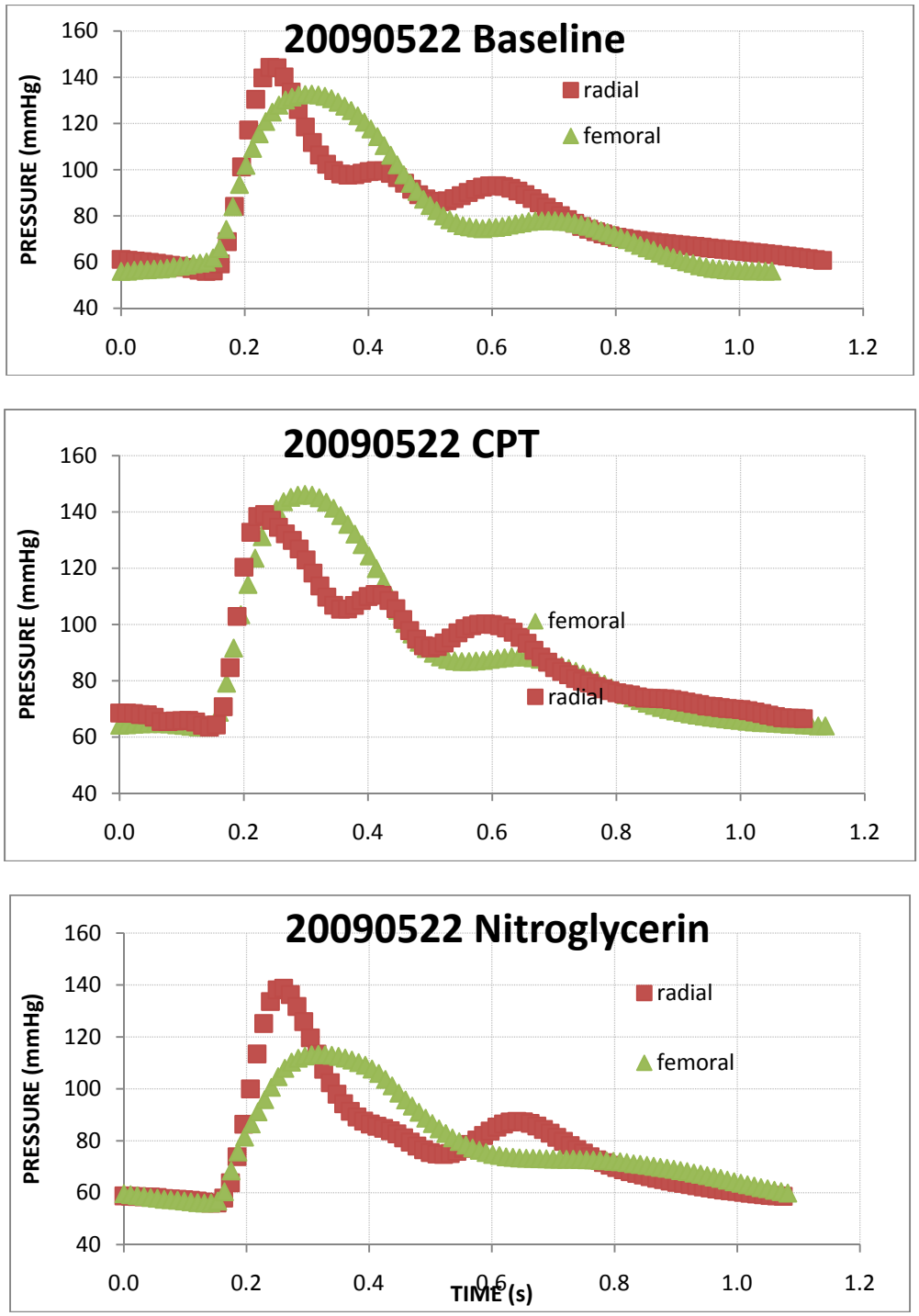

Fig. 4.22: 20090522 Experimental Tonometry Recordings

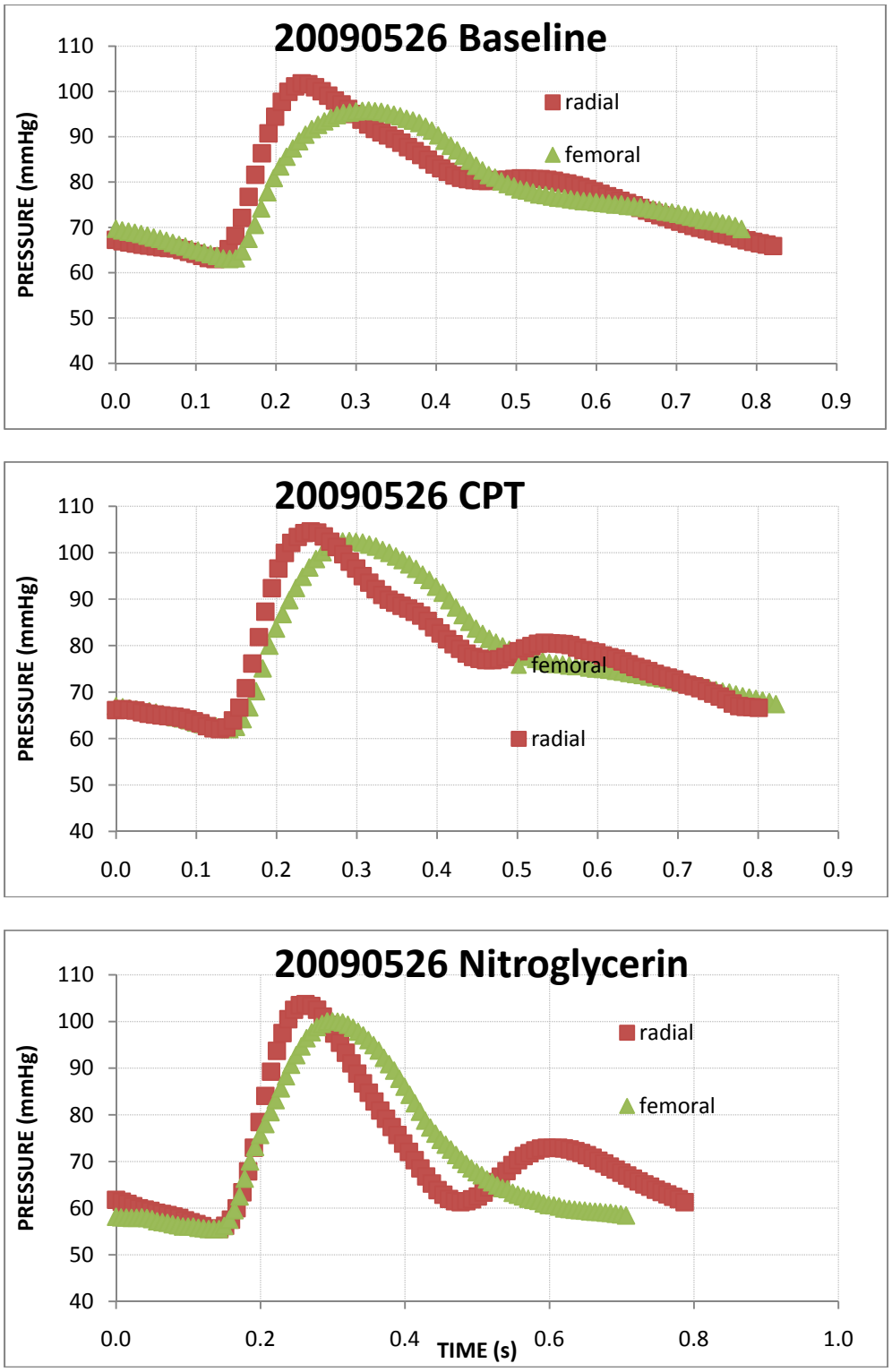

Fig. 4.23: 20090526 Experimental Tonometry Recordings

Modeled Waveforms

Figure 4.24, below, shows measured and predicted pressures in the carotid, radial, and femoral arteries during a CPT test. The carotid pressure was used as the model input, and femoral and radial pressures were predicted. The model parameters were adjusted by the fitting routine to minimize the sum-squared error between the experimental and predicted traces. Note that when evaluating the goodness of the fit, both the root-mean square error and the accuracy of the predicted systolic pressure should be evaluated (from a clinical perspective).

Fig. 4.24: Measured and Modeled Waveforms: Carotid, Radial, & Femoral

Figure 4.25, below, shows measured pressures in the radial artery, and shows measured and predicted pressures in the femoral artery under BSL conditions. The radial pressure was used as the model input, and the femoral artery waveform was predicted. The model parameters reported in the Statistical Analysis and Discussion sections were estimated using this approach (i.e. predicting femoral pressure waveforms from radial artery waveforms).

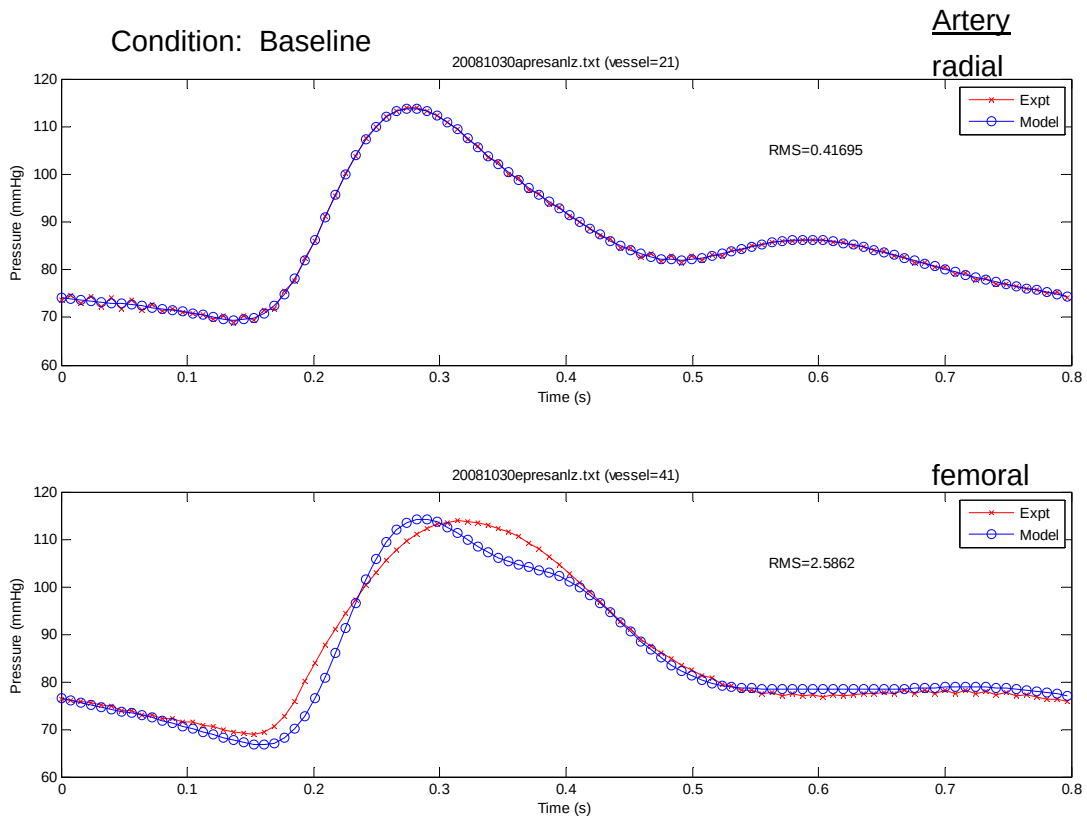

Fig. 4.25: Measured and Modeled Waveforms: Radial, & Femoral

Statistical Analysis

A preliminary analysis of 23 sets of carotid, radial, and femoral recordings from 8 subjects showed that pressure waves predicted by the model had higher sum squared error (SSE), i.e. the fits were worse, when carotid pressure was used as an input than when radial or femoral pressure was used as an input. This analysis is summarized in Table 4.1. The top row of the table shows the difference between the SSEs when carotid or radial artery pressure was used as input (column 1), when femoral or radial was used as input (column 2), and when carotid or femoral was used as input (column 3). The probabilities that the case-by-case SSEs were equal is shown in the bottom row. The hypotheses that the case-by-case SSEs were equal for the first and third columns are therefore rejected. The higher SSEs when carotid artery pressure is used as a model input probably reflects the difficulty in obtaining high-fidelity pressure traces from carotid tonometry, compared to the radial or femoral tonometry.

Table 4.1: Comparison of Model Fit Quality when Different Vessel Inputs are Used

	$SSE_{Carotid}$ - SSE_{Radial}	$SSE_{Femoral}$ - SSE_{Radial}	$SSE_{Carotid}$ - $SSE_{Femoral}$
Mean (Pa^2)	3.5×10^8	1.7×10^8	3.3×10^8
SD (Pa^2)	5.5×10^8	1.2×10^8	5.6×10^8
n	23	23	23
Probability	0.006	0.493	0.010

Due the results of the preliminary analysis described above, carotid recordings were not used in the formulation of the main hypotheses to be tested. The model was

used to predict femoral artery pressure from radial artery pressure. The average root mean square error between the femoral pressure waveforms predicted by the model and the measured femoral pressure waveforms was 6.81 ± 4.46 mmHg. This number is the average of 63 root mean square errors: under baseline, cold pressor test, and nitroglycerin conditions in 21 subjects.

Brachial systolic pressure predicted by the model was significantly correlated ($p<10^{-4}$) with measured brachial systolic pressure, both overall (r=0.67) and during each condition (r=0.90, 0.90, 0.75 under baseline, cold pressor, and nitroglycerin conditions respectively; Table 4.2). Brachial systolic pressure predicted by the model was significantly less than measured, overall and under baseline and cold pressor, but not nitroglycerin, conditions., as shown in Fig. 4.26.

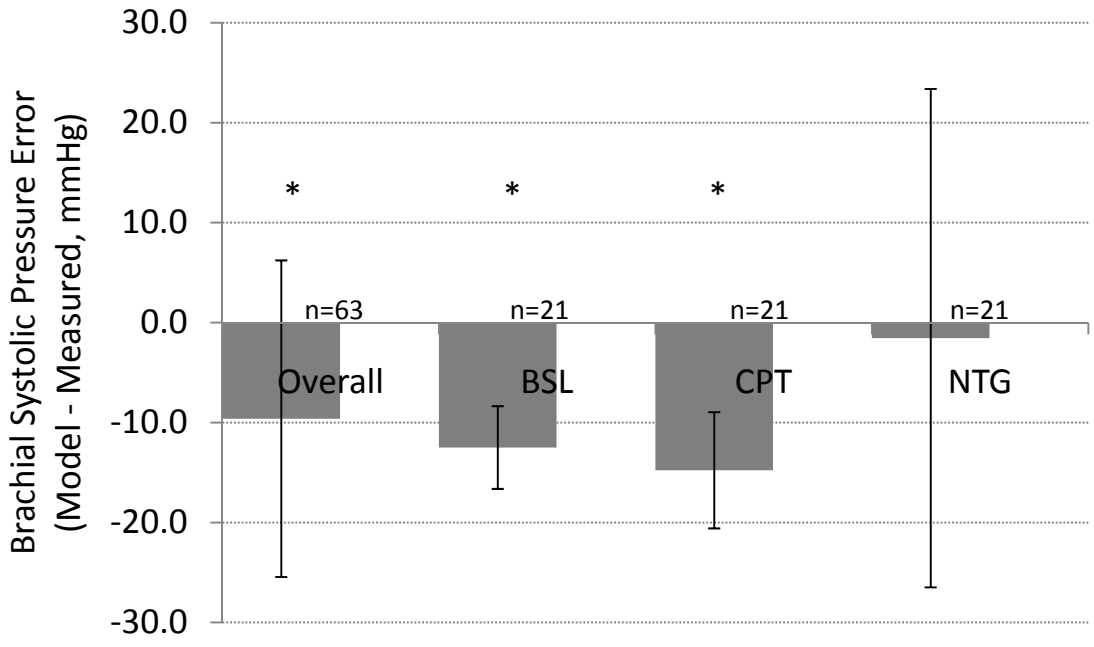

Fig.4.26: Brachial systolic pressure prediction error (mean +- SD). Differences that are significantly different than zero ($p<0.05$, paired t-test) indicated by asterisk.

Table 4.2: Correlation between model and measured brachial systolic pressures

	Overall	BSL	CPT	NTG
n	63	21	21	21
r	0.672	0.899	0.895	0.754
Prob. that r = 0	1.7E-09	5.1E-06	4.4E-08	7.9E-05

A single-factor analysis of variance (ANOVA) was used to determine whether or not the mean values of the fitted model parameters, and other quantities derived from the fitted model parameters, were significantly different for different conditions. The three conditions were baseline (BSL), cold pressor test (CPT), and nitroglycerin (NTG). Eight different variables were analyzed this way: b_1, b_2, a_{mult}, model peripheral resistance (TPR-VR, total peripheral resistance minus venous resistance), model arterial blood volume (Vol), model arterial compliance (Compl), cardiac output (CO), and aortic pressure (AorPres). For each variable, the F statistic and associated probability value were determined, and a $p<0.05$ was accepted as significant. The results are summarized in Table 4.3. The mean values of small vessel diameter (a_{mult}), model peripheral resistance (TPR-VR), model arterial blood volume (Vol), and estimated aortic pressure all were significantly different for different conditions. The mean values of stiffness (b_1), transition radius (b_2), model compliance, and predicted cardiac output did not vary significantly with condition.

After computing the single-factor ANOVA, a further analysis was used to determine which conditions were different from which. The Tukey method was used for this purpose. This method calculates a minimum significant difference in means for two or more sets of data. If the actual difference exceeds this value, the difference in means is considered significant.

Table 4.3: P values for the single factor ANOVA

Variable	P-Value	Significant at 0.05?
b_1	0.465	No
b_2	0.123	No
a_{mult}	0.002	Yes
TPR-VR	0.005	Yes
Vol	0.005	Yes
Compl	0.112	No
CO	0.068	No
Aortic Pressure	0.00007	Yes

Using this test a standard error (SE) is computed using the square root of the sum squared error over the number of data points: $SE = \sqrt{(s^2/n)}$, where n = total number of data points = 63, and s^2 = error mean squared from the ANOVA. (In other words, s^2 = the denominator of the F statistic.)

A q statistic is computed by taking the difference in the means of two data subsets and dividing by the standard error: $q = (Xbar_b - Xbar_a) / SE$. A critical q value is found using a table of critical values. For these data, the critical q value was found using 0.05 level of significance. The degrees of freedom were $df_1 = 3$ (the number of groups), and $df_2 = 60$ (the total data points minus number of groups).

$$q_{critical}(0.05, 3, 60) = 3.399 \quad \text{(Zar, 1984, p. 528)}$$

The means are considered different (with probability $p<0.05$) if the q statistic exceeds the critical value. Table 4.4 shows which pairs of conditions had significantly different means, as determined from the Tukey method, for the variables whose ANOVAs showed significant dependence on condition.

The only model parameter which was significantly different between experimental conditions was the small vessel diameter adjustment factor, a_{mult}, which was greater during NTG than during BSL, and greater during CPT than during BSL (refer to Table 4.3 and Table 4.4). Since a_{mult} is a small vessel diameter scaling factor, these significant differences indicate that the small vessel diameters were largest in the NTG condition. This is a logical result because nitroglycerin is a vasodilator.

The quantity "TPR-VenRes" is the model resistance in the systemic arteries and small vessels, down to the modeled capillaries, hence the name, total peripheral resistance minus venous resistance. The significantly greater TPR-VR under CPT than NTG conditions conforms to expectations: the CPT condition should increase peripheral resistance by causing vasoconstriction, while nitroglycerin should decrease peripheral resistance by causing vasodilation.

The quantity "Vol" is the model blood volume of the systemic arteries and small vessels, down to the modeled capillaries, under the different experimental conditions. The significantly greater blood volume under NTG than BSL and CPT conditions is a reasonable outcome, since vasodilation induced by nitroglycerin will increase the blood volume of these vessels.

The quantity "Compl" is the compliance of the model systemic arteries and small vessels, down to the capillaries, under the different experimental conditions. The difference in compliance estimates between conditions was not significant.

The quantity "CO" is the estimated cardiac output under the different experimental conditions. The difference in cardiac output estimates between conditions was not significant.

The quantity "AorPres" is the estimated mean blood pressure at the aortic root under different experimental conditions. The significantly greater aortic blood pressure under CPT than BSL and NTG conditions is a rational result, since vasoconstriction induced by CPT conditions will apply more force on the blood (from the vessels), thus explaining the observed increase in blood pressure.

Table 4.4: Significant differences found using the Tukey Test

Significant Variables	Significant differences found with Tukey test	q-value
a_{mult}	NTG-BSL	3.598
	NTG-CPT	5.059
TPR-VR	NTG-CPT	4.801
Vol	NTG-BSL	3.505
	NTG-CPT	4.675
AorPres	CPT-BSL	5.109
	NTG-CPT	6.320

Table 4.5 gives the detailed statistical results for the ANOVAs for all eight variables tested, and for the Tukey testing, in the cases where the ANOVAs were

significant. Fig. 4.27 displays the means and standard deviations of the eight predicted model variables, as well as the significant differences between means, when appropriate.

To determine whether the hemodynamic perturbations (CPT and NTG conditions) were sufficient stimuli to test the model's ability to detect vascular changes in vascular parameters, the mean blood pressure (BP) and heart rate (HR) were compared between conditions. Table 4.6 compares the mean BP response, measured via an inflatable cuff at the brachial artery, in response to the different hemodynamic perturbations. After a significant ANOVA (p=6E-06), the BP means were compared by applying a Tukey and a t-Test. The Tukey-test found a significantly higher mean BP under CPT conditions compared to NTG and BSL conditions, but no significant difference in mean BP between NTG and BSL conditions. However, a two-tailed t-test found a significant difference in mean BP between NTG and BSL conditions (P=0.0007). Table 4.7 compares the mean HR between conditions. The ANOVA was not significant (p=0.844).

Table 4.5.A: Stiffness (b_1, Pa)

***b_1* (Pa) SUMMARY**

Groups	*Count*	*Sum*	*Average*	*Variance*
BSL	21	28241073	1344800	6.72E+11
CPT	21	24785896	1180300	6.78E+11
NTG	21	30877603	1470400	3.7E+11

ANOVA

Source of Variation	*SS*	*df*	*MS*	*F*	*P-value*
Between Groups	8.88864E+11	2	4.44E+11	0.775	0.4651
Within Groups	3.4394E+13	60	5.73E+11		
Total	3.52829E+13	62			

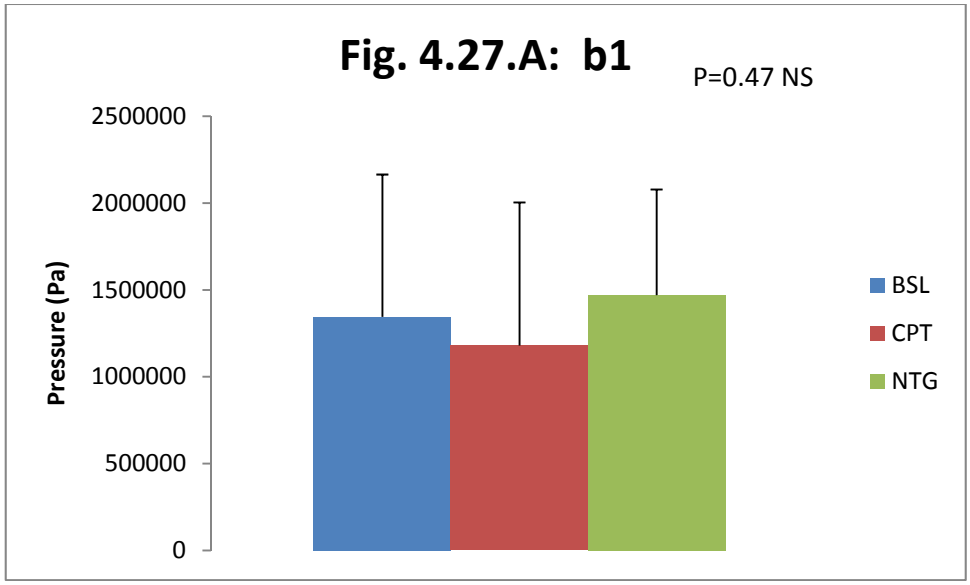

Table 4.5.B: Transition radius (b_2, cm)

***b_2* (cm) SUMMARY**

Groups	*Count*	*Sum*	*Average*	*Variance*
BSL	21	6.91113	0.329	0.1897
CPT	21	8.20815	0.391	0.1950
NTG	21	3.08575	0.147	0.0811

ANOVA

Source of Variation	*SS*	*df*	*MS*	*F*	*P-value*
Between Groups	0.675473	2	0.337736	2.175	0.1225
Within Groups	9.318994	60	0.155317		
Total	9.994467	62			

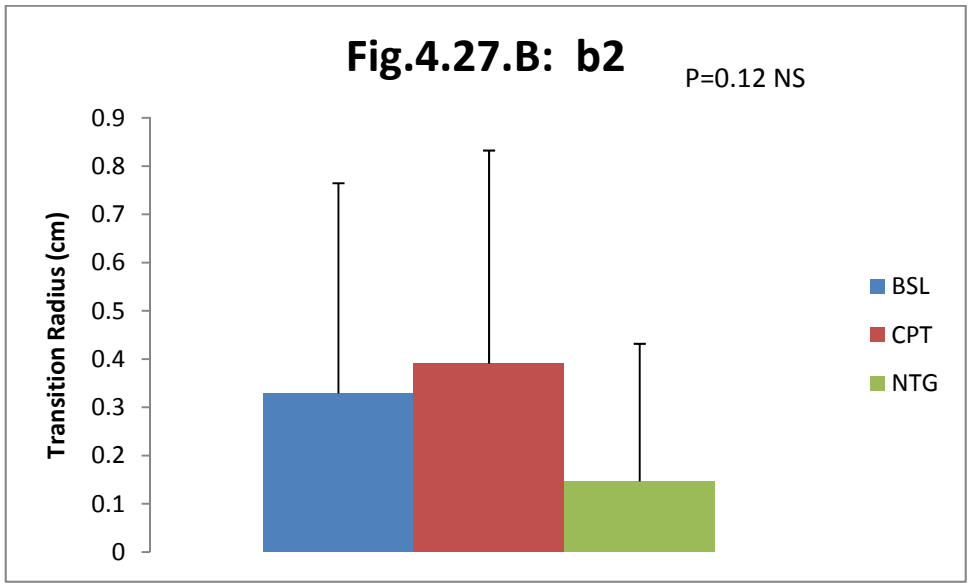

Table 4.5.C: Small vessel diameter adjustment factor (a_{mult}, dimensionless)

a_{mult} SUMMARY

Groups	*Count*	*Sum*	*Average*	*Variance*
BSL	21	7.045	0.335476	0.02594
CPT	21	5.552	0.264381	0.030529
NTG	21	10.719	0.510429	0.092529

ANOVA

Source of Variation	*SS*	*df*	*MS*	*F*	*P-value*
Between Groups	0.673416	2	0.336708	6.779	0.0022
Within Groups	2.979963	60	0.049666		
Total	3.653379	62			

Tukey Multiple Comparisons tests

SE	0.048632
q(CPT-BSL)	1.4619
q(NTG-BSL)	3.5975
q(NTG-CPT)	5.0594
ν	60
k	3
q_crit	3.399

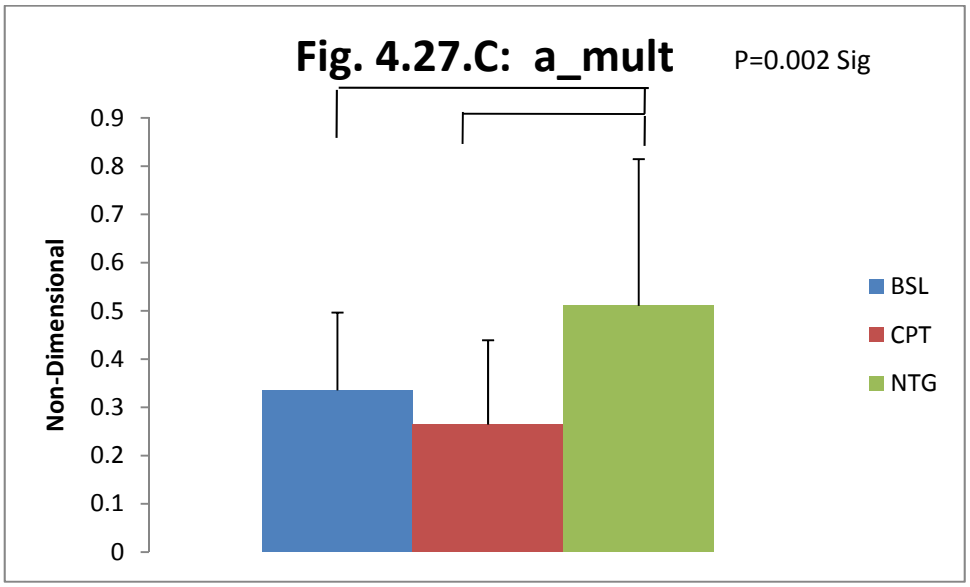

Table 4.5.D: Model peripheral resistance (TPR-VR, Pa-s/mL)

TPR-VR (Pa-s/mL) SUMMARY

Groups	*Count*	*Sum*	*Average*	*Variance*
BSL	21	1860.1	88.58	589.7
CPT	21	2166.6	103.17	1490.0
NTG	21	1520.7	72.41	506.2

ANOVA

Source of Variation	*SS*	*df*	*MS*	*F*	*P-value*
Between Groups	9941.61	2	4970.805	5.766	0.0051
Within Groups	51719.05	60	861.9841		
Total	61660.66	62			

Tukey Multiple Comparisons tests

SE	6.406783
q(CPT-BSL)	2.2781
q(NTG-BSL)	2.5226
q(NTG-CPT)	4.8007
ν	60
k	3
q_crit	3.399

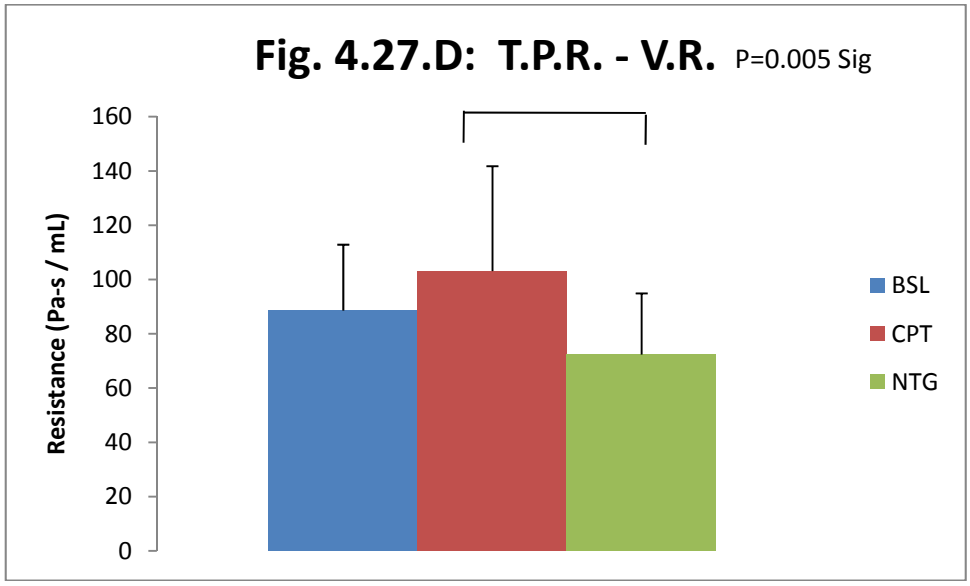

Table 4.5.E: Model arterial blood volume (Vol, mL)

Volume (mL) SUMMARY

Groups	*Count*	*Sum*	*Average*	*Variance*
BSL	21	30083	1432	33006
CPT	21	28483	1356	36507
NTG	21	34876	1660	197622

ANOVA

Source of Variation	*SS*	*df*	*MS*	*F*	*P-value*
Between Groups	1054021	2	527010.3	5.918	0.0045
Within Groups	5342724	60	89045.4		
Total	6396744	62			

Tukey Multiple Comparisons tests

SE	65.11726
q(CPT-BSL)	1.1701
q(NTG-BSL)	3.5050
q(NTG-CPT)	4.6751
ν	60
k	3
q_crit	3.399

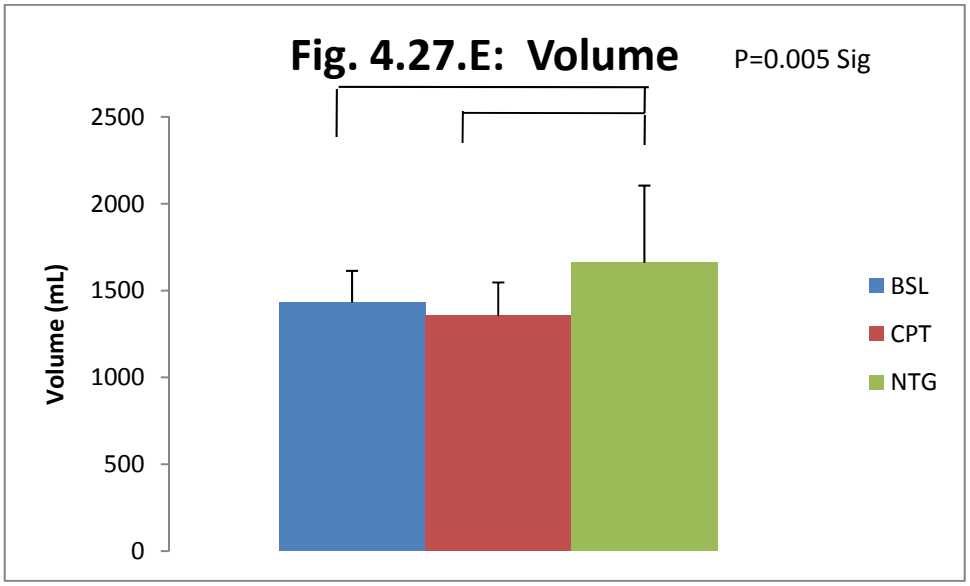

Table 4.5.F: Model arterial compliance (Compl, mL/mmHg)

Compliance (mL/mmHg) SUMMARY

Groups	*Count*	*Sum*	*Average*	*Variance*
BSL	21	23.799	1.133286	0.324999614
CPT	21	18.715	0.89119	0.031538162
NTG	21	23.877	1.137	0.1932861

ANOVA

Source of Variation	*SS*	*df*	*MS*	*F*	*P-value*
Between Groups	0.833324	2	0.416662	2.273	0.1118
Within Groups	10.99648	60	0.183275		
Total	11.8298	62			

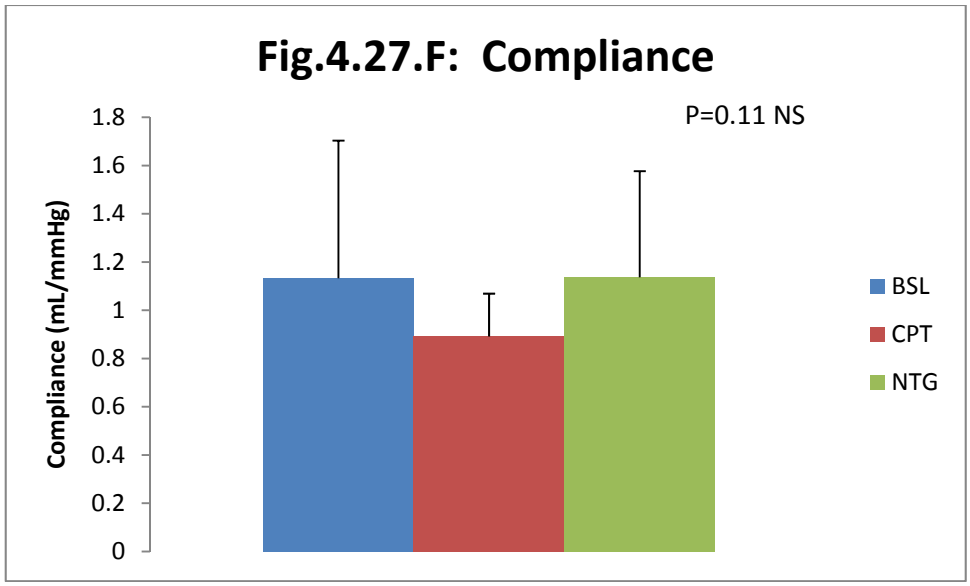

Table 4.5.G: Estimated cardiac output (C.O., L/min)

CO (L/min) SUMMARY

Groups	*Count*	*Sum*	*Average*	*Variance*
BSL	21	141.63	6.74	3.15
CPT	21	140.60	6.70	2.43
NTG	21	171.60	8.17	10.14

ANOVA

Source of Variation	*SS*	*df*	*MS*	*F*	*P-value*
Between Groups	29.51848	2	14.75924	2.817	0.0677
Within Groups	314.3331	60	5.238885		
Total	343.8516	62			

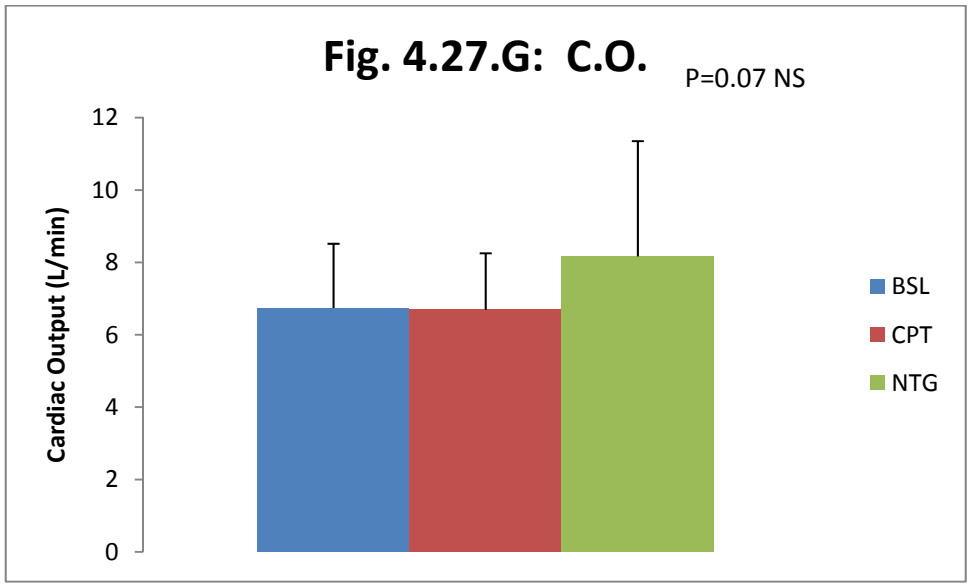

Table 4.5.H: Estimated aortic pressure (mmHg)

Aortic Pressure (mmHg) SUMMARY

Groups	*Count*	*Sum*	*Average*	*Variance*
BSL	21	1786.8	85.08571	46.09329
CPT	21	1993.1	94.90952	113.6239
NTG	21	1737.9	82.75714	73.20657

ANOVA

Source of Variation	*SS*	*df*	*MS*	*F*	*P-value*
Between Groups	1747.269	2	873.6344	11.252	0.000071
Within Groups	4658.475	60	77.64125		
Total	6405.744	62			

Tukey Multiple Comparisons tests

SE	1.922811
q(CPT-BSL)	5.1091
q(NTG-BSL)	1.2110
q(NTG-CPT)	6.3201
ν	60
k	3
q_crit	3.399

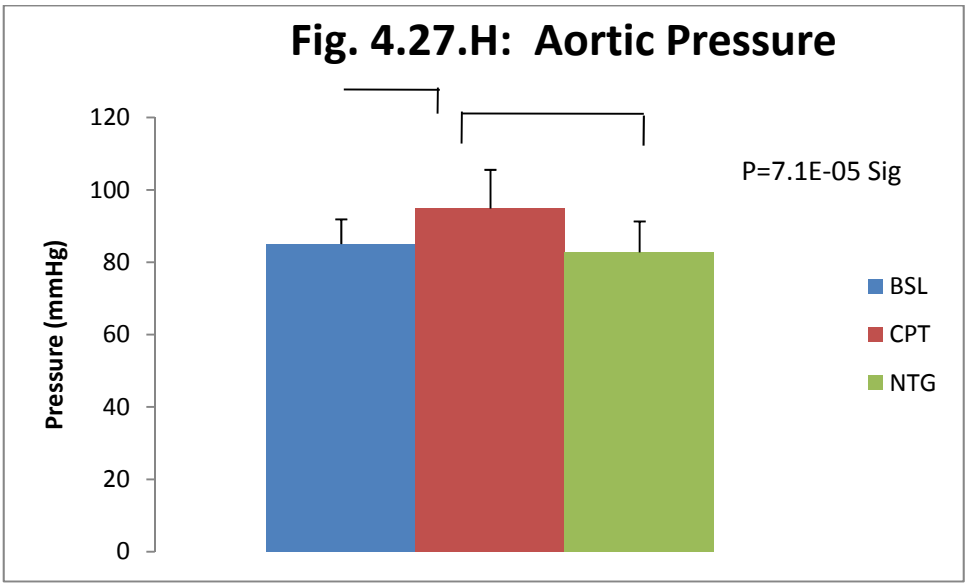

Table 4.6: Mean blood pressure under different conditions

Brachial Cuff Mean Blood Pressure

Group	*n*	*Average (mmHg)*	*Variance ($mmHg^2$)*
BSL	21	81.4	42.9
CPT	21	91.1	119.0
NTG	21	77.1	58.2

ANOVA

Source of Variation	*SS*	*df*	*MS*	*F*	*P-value*
Between Groups	2170.1	2	1085.1	14.790	6E-06
Within Groups	4401.7	60	73.4		
Total	6571.8	62			

Tukey testing: multiple comparisons

	CPT-BSL	NTG-BSL	CPT-NTG
Mean Difference (mmHg)	+9.7	-4.3	+14.0
P < 0.05?	YES	No	YES

Table 4.7: Heart rate under different conditions

HR (bpm)

Group	*n*	*Average (bpm)*	*Variance (bpm^2)*
BSL	21	61.1	141.5
CPT	21	62.7	134.2
NTG	21	63.2	169.0

ANOVA

Source of Variation	*SS*	*df*	*MS*	*F*	*P-value*
Between Groups	50.4	2	25.2	0.170	0.844
Within Groups	8894.3	60	148.2		
Total	8944.7	62			

(No multiple comparisons tests because ANOVA not significant.)

Chapter 5

DISCUSSION

The model displayed good predictive capability in some regards, and a lack of sensitivity in other regards. Predicted and measured brachial systolic pressures were significantly correlated, both overall and under each experimental condition, although predicted brachial systolic pressure was significantly less than measured overall and under baseline and cold pressor conditions. These correlations under all conditions suggest the model is detecting changes in systolic blood pressure, although it is not predicting the absolute pressure completely accurately.

To assess whether the hemodynamic perturbations caused by the cold pressor test and nitroglycerin were sufficient stimuli to test the model's ability to detect vascular changes in vascular parameters, the mean blood pressure (BP) and heart rate (HR) were compared between conditions (Tables 4.6 and 4.7). The significantly higher mean BP under CPT compared to NTG and BSL indicates the CPT perturbation was a sufficient stimulus to test the model. However, the lack of significant difference in BP between the NTG and BSL conditions suggests the NTG condition may not have been a sufficient vascular stimulus. The use of 0.3 mg nitroglycerin rather than a higher dose was intended to eliminate the possibility of severe hypotension that could have required medical intervention, and it succeeded in this regard. However, it may have been overly cautious, particularly in this population of young healthy subjects, whose baroreflexes

apparently enabled them to compensate well for the vasodilatory effects of the drug. The lack of significant difference in HR between conditions is also interesting. In the case of the CPT, the painful stimulus will tend to be sympathoexcitatory, thus raising HR and blood pressure. However, the increase in BP will cause a baroreflex-mediated fall in HR. These opposite effects apparently cancelled each other out. Nitroglycerin has no significant direct effect on HR, but the vasodilation and fall in blood pressure it causes usually leads to a baroreflex-mediated rise in HR. In fact, the mean HR was higher during NTG than during BSL or CPT, but the differences were not significant, perhaps due to the conservative does of NTG used. Thus, it is possible that the model's lack of sensitivity in detecting changes in some of the vascular properties was due to a lack of strong stimuli.

Parameter a_{mult} was significantly greater under NTG than BSL and CPT conditions. Since a_{mult} is a small vessel diameter scaling factor, these significant differences indicate that small vessel diameters were largest in the NTG condition. This is a logical result since nitroglycerin is a vasodilator. Thus the model is capturing this vascular property change under varying hemodynamic conditions. The model did not detect changes in parameter b_1 (refer to Table 4.2 and Table 4.3), which represents small vessel stiffness, when hemodynamic perturbations were applied. Under CPT conditions, b_1 might be expected to increase in response to sympathetic activation, while under NTG conditions, b_1 might be expected to decrease due to vasculature relaxation. With regard to parameter b_2, which represents the transition radius between large and small vessels, the model found no significant difference under the varying hemodynamic conditions.

To the best of our knowledge, no previous literature has characterized the response of b_2 to hemodynamic perturbations.

The quantity "TPR-VenRes", total peripheral resistance minus venous resistance, is the resistance in the systemic arteries and small vessels, down to the modeled capillaries. The model found a significantly greater TPR-VR under CPT than NTG conditions. This is an expected result since the CPT condition should increase peripheral resistance via sympathetic activation causing vasoconstriction, while nitroglycerin should decrease peripheral resistance by causing vasodilation. Thus the model is capturing the expected change in TPR-VR under varying hemodynamic conditions. Note that the consistent significant differences found in parameter a_{mult} and TPR under similar conditions is logical since TPR is directly dependent on small vessel diameter. The quantity "Compl" is the compliance of the model systemic arteries and small vessels, down to the capillaries, under the different experimental conditions. The lack of significant difference in the model estimates of compliance under varying hemodynamic conditions suggests the model is not detecting changes in this property. Similar to parameter b_1, compliance might be expected to increase in response to sympathetic activation, while under NTG conditions, compliance might be expected to decrease due to vasculature relaxation. This finding is consistent with our other findings, since these overall arterial compliance model estimates are dependent on the model estimates of parameters b_1 and b_2, which were also found not to be significantly different under varying hemodynamic conditions.

The quantity "AorPres" is the mean blood pressure in the aorta under the different experimental conditions. The significantly greater aortic blood pressure model estimate under CPT than BSL and NTG conditions is an expected result, since sympathetically-activated vasoconstriction induced by CPT conditions will apply more force on the blood (from the vessels). Thus the model is capturing the expected change in aortic blood pressure under CPT conditions. However, under NTG conditions aortic blood pressure is expected to be significantly lower than under BSL conditions, but such a difference was not detected by the model. Model estimates of cardiac output (CO) were not different under NTG conditions. Under CPT conditions, CO is affected by conflicting factors. While sympathetic activation will increase cardiac contractility, which would increase CO under CPT conditions, increased peripheral resistance via sympathetic activation would decrease CO. Thus the insignificant change in the CO model estimate upon the application of CPT conditions is not surprising.

Other studies have also predicted blood pressure noninvasively from radial artery tonometry measurements. Chen C, Nevo E, Fetics B, Pak PH, Yin FCP, Maughan WL, Kass DA, 1997 (described in the introduction) estimated central arterial pressures to 0.2 ± 3.8 mmHg error (compared to directly measured central intra-arterial pressures). However, this quantity is not directly comparable with our error of 6.81 ± 4.46 mmHg, since we compared noninvasive predictions to noninvasive measurements. Moreover, the potentially most valuable capability of our model lies not in its ability to accurately predict pressure, but rather in its ability to generate vascular parameter estimates specific to an individual, yielding potentially valuable information about the patient's vasculature.

Due to the lack of quality of the carotid artery tonometry recordings, model parameters could not be sufficiently and reliably constrained when these recordings were included in the modeling process, thus they were not included. Additionally, a comparison of the error of using different tonometry recording sites as input to the model (to predict pressures at other sites) was conducted (see Table 4.1). A significantly larger error was found when using the carotid artery site for input to the model relative to the radial and femoral artery sites, suggesting carotid artery tonometry recordings are more prone to error. This confirms the observation of Chen C, Nevo E, Fetics B, Pak PH, Yin FCP, Maughan WL, Kass DA, 1997 that the carotid artery is not ideal for applanation tonometry, because it is encompassed by loose tissue and is affected by breathing.

A limitation of this study was the lack of simultaneously recorded tonometry signals at the different sites of applanation. This is particularly a concern during the perturbations (i.e. the cold pressor test and nitroglycerin administration), because the vasculature properties are likely rapidly changing in response to the stimuli. This hinders the comparison of waveforms at different applanation sites within and between conditions. Future investigations should implement simultaneous acquisition of the tonometry signals at different recording sites to avoid this limitation.

With regard to the 6.81 ± 4.46 mmHg error of our pressure predictions, direct invasive measurements are recommended to compare to our noninvasively predicted waveforms. This will help determine whether our error is due to a flaw in our modeling approach, or to the error associated with noninvasive measurements. Cohn JN et al., 1995 describes the reduced sensitivity of noninvasive tonometry measurements, which tended to result in a damped waveform with less oscillatory components relative to an

invasively measured waveform. Further, this study quantifies a pressure error difference (invasive minus noninvasive) measurement between brachial intra-arterial and radial artery tonometry waveforms: 5.0 ± 4.9 mmHg for mean pressure, 9.2 ± 8.5 mmHg for systolic pressure, and 0.6 ± 6.1 mmHg for diastolic pressure. Some of this difference is likely due to pressure amplification between the brachial and radial artery recording sites. Nonetheless, these pressure error differences between invasive and noninvasive measurements, although closely correlated, are within the pressure error predicted by our model. Thus it is possible that the error of our modeled pressure predictions is, to an extent, due to the error associated with noninvasive measurements.

In conclusion, the model has shown potential to capture changes in vascular properties induced by hemodynamic perturbations, as reflected by changes in the model parameters. These vascular parameter estimates are specific to the individual, and yield potentially valuable information about the patient's vasculature, which is a unique feature of our model. Another distinctive capability of our model is its ability to use pressure waveforms from any vessel site to predict pressure and flow waveforms everywhere else in the systemic arterial circulation.

Specific Aim

The specific aim of this study was to predict blood pressure waveforms throughout the arterial network using noninvasive measurements and computational modeling.

Hypotheses

1. *The model will be capable of predicting blood pressure waveforms at the femoral artery from radial artery recordings to within a root mean-squared error of 5 mmHg under varying hemodynamic conditions.*

Evaluation: Hypothesis 1 was rejected; the model predicted blood pressure waveforms at the femoral artery from radial artery recordings with a root mean-squared error of 6.81 ± 4.46 mmHg under varying hemodynamic conditions.

2. *Changes in vascular properties induced by nitroglycerin and the cold pressor test will cause changes in estimated model parameters.*

Evaluation: Hypothesis 2 was partially accepted. The model parameter a_{mult} was significantly greater under NTG than BSL and CPT conditions (refer to Table 4.2 and Table 4.3). a_{mult} is a small vessel diameter scaling factor, thus these significant differences indicate that small vessel diameters were largest in the NTG condition. This is a logical result since nitroglycerin is a vasodilator. Thus the model is capturing this vascular property change during these perturbations. With regard to the comparison of the fitted model parameter b_1 under varying hemodynamic conditions, the lack of a significant difference ($p>.05$) with the application of CPT and NTG conditions indicates the model is not detecting vasculature property changes during these perturbations. Compared to BSL conditions, the CPT and NTG conditions are expected to increase and decrease vascular stiffness, respectively, via increased and decreased vascular tone, respectively. Thus this lack of model sensitivity suggests future model refinement is necessary.

Future Investigations

The model has many aspects which deserve further investigation. First, the arterial radii are not currently adjusted for different individuals. One method to address this concern would be to scale the aortic radius r_{ao} based on the individual's mass M, according to universal scaling laws (West GB, 1999):

$$r_{ao} \sim M^{3/8} \tag{4}$$

Using this adjusted aortic radius estimate as the input, the downstream arterial radii would scale according to equations 1 and 2. Yet even with this adjustment, one would expect different anatomical geometries depending on the individual's body composition. Thus a dual energy X-ray absorptiometry (DXA) scan may provide an additional resource to scale arterial radii specific to an individual's body composition. Alternatively, another method to scale arterial radii specific to an individual would be to measure the individual's carotid artery diameter via ultrasound imaging, and use this estimate as an input to scale the arterial network according to equations 1 and 2. However, concerns over the accuracy of ultrasound imaging to determine an absolute diameter have presently deterred the incorporation of this approach.

When indexing arterial stiffness in large arteries, several approaches other than parameter optimization may yield more accurate estimates. One method to derive an estimate of the stiffness of the large arteries would be to use a PWV value (McDonald DA, 1974):

$$PWV = \sqrt{\frac{\beta}{2\rho}} \quad \therefore \quad \beta = PWV^2 \cdot 2\rho \tag{5}$$

where ρ is the density of blood, approximately a constant of 1.05 kg/L (Hinghofer-Szalkay & Greenleaf, 1987).

With regard to data acquisition, the studies by (Chen, et al., 1997) and by (Cohn, et al., 1995) relied on arterial tonometer sensor arrays, which adjust the probe position and applanation pressure, to obtain a theoretically optimal waveform. Our experimental approach relied on a tonometer pencil-tipped probe clamped in place and applied to the

artery recording site of interest. A study comparing the effectiveness of the two techniques would provide insight into which technique is superior to obtain an optimal waveform via tonometry.

Finally, intra-arterial recordings would be ideal for comparison to the waveforms predicted by the model. However, such recordings carry significant risk to the patient and are not feasible outside of a clinical catheterization lab. Future collaborations with Christiana Hospital in Newark, Delaware, may offer access to this extremely valuable resource.

REFERENCES

Carew, T., Vaishnav, R., & Patel, D. (1968). Compressibility of the Arterial Wall. *Circ Res , 23(1)*, 61-68.

Center for Disease Control and Prevention. (n.d.). *Heart Disease*. Retrieved 03 26, 2009, from http://www.cdc.gov/heartdisease/

Chen, C., Nevo, E., Fetics, B., Pak, P., Yin, F., Maughan, W., et al. (1997). Estimation of Central Aortic Pressure Waveform by Mathematical Transformation of Radial Tonometry Pressure. *Circulation , 95*, 1827-1836.

Cohn, J., Finkelstein, S., McVeigh, G., Morgan, D., Lemay, L., Robinson, J., et al. (1995). Noninvasive Pulse Wave Analysis for the Early Detection of Vascular Disease. *Hypertension , 26*, 503-508.

deTombe, P., Jones, S., Hunter, W., Burkhoff, D., & Kass, D. (1993). Ventricular stroke work and efficiency remain nearly optimal despite broad changes in ventricular-vascular coupling. *Am J Physiol , 264*, H1817-H1824.

Fetics, B., Nevo, E., Chen, C., & Kass, D. (1999). Parametric Model Derivation of Transfer Function for Noninvasive Estimation of Aortic Pressure by Radial Tonometry. *IEEE Trans. Biomed. Engin. , 46*, 698-706.

Girerd, X. (1991). Arterial distensibility and left ventricular hypertrophy in patients with sustained essential hypertension. *Am Heart J , 122*, 1210-1214.

Hinghofer-Szalkay, H., & Greenleaf, J. (1987). Continuous Monitoring of Blood Volume Changes in Humans. *J. Appl. Physiol. , 63*, 1003-7.

Kass DA, B. R. (1991). Evaluation of contractile state by maximal ventricular power divided by the square of end-diastolic volume. *Circulation , 84*, 1698-1708.

Kass, D., Maughan, W., Guo, Z., Kono, A., Sunagawa, K., & Sagawa, K. (1987). Comparative influence of load versus inotropic states on indexes of ventricular contractility: experimental and theoretical analysis. *Circulation , 76*, 1422-1436.

Laurent et al. (2006). Expert consensus document on arterial stiffness: methodological issues and clinical applications. *European Heart Journal , 27*, 2588-2605.

Laurent, S., Boutouyrie, P., Asmar, R., Gautier, I., Laloux, B., Guize, L., et al. (2001). Aortic stiffness is an independent predictor of all-cause and cardiovascular mortality in hypertensive patients. *Hypertension , 37*, 1236-1241.

Levy, D., Garrison, R., Savage, D., Kannel, W., & Castelli, W. (1990). Prognostic implications of echocardiographically determined left ventricular mass in the Framingham Heart Study. *N Engl J Med , 322*, 1561-1566.

McDonald DA. (1974). *Blood Flow in Arteries.* Williams & Wilkins.

Nichols, W. (2005). Clinical measurement of arterial stiffness from noninvasive pressure waveforms. *Am. J. Hypertension* , 18: 3S-10S.

Nichols, W., & Edwards, D. (2001). Arterial Elastance and Wave Reflection Augmentation of Systolic Blood Pressure. *J. Cardiovasc. Pharm. Ther. , 6*, 5-21.

Nichols, W., Estrada, J., Braith, R., Owens, K., & Conti, C. (2006). Enhanced external counterpulsation treatment improvesarterial wall properties and wave reflection characteristics in patients with refractory angina. *J. Am. College Cardiology* , 48: 1208-1214.

Nichols, W., O'Rourke, M. A., Yaginuma, T., Murgo, J., Pepine, C., & Conti, C. (1985). Effects of age on ventricular-vascular coupling. *Am. J. Cardiol.* , 55: 1179-1184.

O'Rourke, M., & Taylor, M. (1967). Input impedance of the systemic circulation. *Circ. Res.* , 20: 365-380.

Ottesen JT, Olufsen MS, Larsen JK. (2004). *Applied Mathematical Models in Human Physiology.* Society for Industrial and Applied Mathematics.

Ottesen, J., Olufsen, M., & Larsen, J. (2004). *Applied Mathematical Models in Human Physiology.* Society for Industrial and Applied Mathematics.

Rose, WC; Johnson, DA; Spaeth, JR; Edwards, J; Beris, AN. (2008). Computational and experimental investigations of arterial hemodynamics. *ASME International Mechanical Engineering Congress and Exposition* (pp. 1-8). Boston: A.S.M.E.

Ross, R. (1981). Atherosclerosis: a problem of the biology of arterial wall cells and their interactions with blood components. *Arteriosclerosis , 1*, 293-311.

Spaeth, J. (2006). An input-parameter model for predicting blood flow and pressure in the human circulatory system. *Undergraduate thesis submitted to the Department of Chemical Engineering, University of Delaware* .

West GB. (1999). The Origin of Universal Scaling Laws in Biology. *Physica A , 263*, 104-113.

West, G. (1999). The Origin of Universal Scaling Laws in Biology. *Physica A , 263*, 104-113.

Williams, B., Lacy, P., Thom, S., Cruickshank, K., Stanton, A., Collier, D., et al. (2006). Differential Impact of Blood Pressure–Lowering Drugs on Central Aortic Pressure and Clinical Outcomes. *Hypertension , 113*, 1213-1225.

Womersley J. (1957). Oscillatory flow in arteries: The constrained elastic tube as a model of arterial flow and pulse transmission. *Phys. Med. Biol. , 2*, 178-187.

Zar, J. (1984). *Biostatistical Analysis* (2nd ed.). Englewood Cliffs, NJ: Prentice-Hall.